REPORT DOCUMENTATION PAGE

Public reporting burden for this collection of information is estimated to average 1 hour per response, including the time for reviewing instructions, searching existing data sources, gathering and maintaining the data needed and completing and reviewing the collection of information. Send comments regarding this burden estimate or any other aspect of the collection of information, including suggestions for reducing the burden to Washington Headquarters Services, Directorate for Information Operations and Reports, 1215 Jefferson Davis Highway, Suite 1204, Arlington, VA 22202-4302 and to the Office of Management and Budget, Paperwork Reduction Project (0704-0188), Washington, DC 20503

1. AGENCY USE ONLY (Leave blank)	2. REPORT DATE April 15, 1997	3. REPORT TYPE AND DATES COVERED Quarter --- Dec. 1, 1996 through Feb. 28, 1997

4. TITLE AND SUBTITLE OF REPORT Visible Light Emitting Materials and Injection Devices	5. FUNDING NUMBERS ONR Grant N00014-92-J-1895

6. AUTHOR(S)

Paul H. Holloway

7. PERFORMING ORGANIZATION NAME(S) AND ADDRESS(ES) Department of Materials Science and ENgineering University of Florida P.O. Box 116400 Gainesville, FL 32611-6400	8. PERFORMING ORGANIZATION REPORT NUMBER: N/A

9. SPONSORING/MONITORING AGENCY NAME(S) AND ADDRESS(ES) Office of Naval Research 800 North Quincy Street Arlington, VA 22217-5000	10. SPONSORING/MONITORING AGENCY REPORT NUMBER:

11. SUPPLEMENTARY NOTES:

12a. DISTRIBUTION AVAILABILITY STATEMENT Unlimited DISTRIBUTION STATEMENT A Approved for public release; Distribution Unlimited	12b. DISTRIBUTION CODE

13. ABSTRACT (Maximum 200 words)

Progress in report on research into ZnSe-based and GaN-based materials and devices for light emitting diodes and diode lasers at blue-green visible wavelengths.

19970509 034

14. SUBJECT TERMS Zinc Selenide Diode Lasers Gallium Nitride Light Emitting Diodes	15. NUMBER OF PAGES: 45
	16. PRICE CODE

17. SECURITY CLASSIFICATION OF REPORT: None	18. SECURITY CLASSIFICATION OF THIS PAGE None	19. SECURITY CLASSIFICATION OF ABSTRACT None	20. LIMITATION OF ABSTRACT None

Quarterly Progress Report

December 1, 1996 to February 28, 1997

Visible Light Emitting Materials and Injection Devices

ONR/DARPA URI

Grant Number N00014-92-J-1895

Prepared by:

Paul H. Holloway
Department of Materials Science and Engineering
University of Florida
P.O. Box 116400
Gainesville, FL 32611
Ph: 352/392-6664; FAX: 352/392-4911
E-Mail: Internet - pholl@silica.mse.ufl.edu

Participants:
University of Florida
Kevin Jones
Robert Park
Joseph Simmons
Cammy Abernathy
Stephen Pearton
Dept. Materials Science and Engineering
Timothy Anderson
Dept. of Chemical Engineering
Peter Zory
Dept. of Electrical Engineering

(I)   Growth by MBE and Characterization of GaN (Robert Park)

III-V Nitride Work

The work performed in this quarter is best described in the attached paper (Appendix I) entitled, "On the kinetics of growth of highly-defective GaN epilayers and the origin of the deep trap responsible for the yellow-band luminescence." This paper has been submitted to Applied Physics Letters.

(II)   Growth and processing of GaN-based materials (Cammy Abernathy and Steve Pearton)

a. Thermal Stability of Hydrogen in $LiAlo_2$ and $LiGaO_2$

Lithium aluminate ($LiAlO_2$) and lithium gallate ($LiGaO_2$) single crystals are attracting attention as substrates for epitaxial growth of GaN and other III-nitrides.[1] Pulsed operation of GaN/InGaN blue laser diodes has been reported for films grown on c-axis sapphire where facets were formed by dry etching,[2] and on a-plane sapphire where facets were formed by cleaving.[3] The lattice mismatch for GaN grown on sapphire is 13.6%, which produces columnar growth in most cases, with defect densities in the 10^9 and $10^{10} cm^{-2}$ ranges.[4] GaN has also been grown on 3C-SiC (3.1% mismatch)[4-7] and on ZnO (2.2% mismatch)[8] substrates, both of which have cubic symmetry and are easily cleaved. The largest bulk GaN crystals that are currently available are typically 5x10 mm^2, produced by high pressure solution growth (20 kbar at ~1600°C),[9] $LiAlO_2$ and $LiGaO_2$ have oriented a-axis lattice constants of 0.3134 and 0.3186 nm, respectively, which translate into mismatches with GaN of -1.5% for $LiAlO_2$ and +0.2% for $LiGaO_2$. Initial studies of growth of III-nitride epilayers on these oxide substrates have shown excellent results for deposition temperatures below 900°C.[10] At higher temperatures, surface degradation is apparent under some conditions, especially when hydrogen is present in the growth ambient. Because NH_3 is the most commonly used source of nitrogen for metalorganic chemical vapor deposition, and metalorganics such as $(CH_3)_3Ga$ produce hydrogen during decomposition, it is clearly important to understand the thermal behavior and stability of hydrogen in $LiAlO_2$ and $LiGaO_2$.

We report on measurements of hydrogen incorporation in both $LiAlO_2$ and $LiGaO_2$ during ^2H plasma treatment and about the thermal stability of implanted hydrogen (as ^2H). In the latter case, outdiffusion begins at about 400°C and is completed by about 700°C, whereas in sapphire, temperatures up to 1000°C have little effect on implanted ^2H depth distributions. High densities of hydrogen ($>10^{20}$ cm^{-3} in $LiAlO_2$ and $>10^{19}$ cm^{-3} in $LiGaO_2$) are incorporated during plasma exposure at 250°C.

Undoped crystals were grown using the Czochralski technique, with diameter 1.5 inch, and orientation (100), for both materials. Hall measurements showed high resistivity ($>10^8$ Ωcm) as expected for such wide bandgap materials (~6 eV). Wafers were polished on one side using a combination of mechanical and chemical treatments. To facilitate measurements of hydrogen incorporation and thermal stability, we introduced the ^2H isotope of hydrogen (which can be detected with better sensitivity using secondary ion mass spectrometry (SIMS) than for ^1H, by two different methods. In the first method, ^2H ions were implanted at 100keV to a

fluence of 2×10^{15} cm^{-2}. Sections of this sample were subsequently annealed at temperatures up to 700°C for 10 min, and SIMS depth profiling was performed for each temperature. In the second method, pieces were exposed to electron cyclotron resonance (ECR) ^{2}H plasmas for 1 h at 250°C. The microwave power was 750 W, and the process pressure was 10 mTorr. SIMS measurements were again carried out before and after a subsequent anneal at 500°C for 1 min under N$_2$.

Depth profiles of ^{2}H for as-implanted and annealed LiAlO$_2$ (a) and LiGaO$_2$ (b) are shown in Fig. II.a.1. In the as-implanted samples, the ^{2}H peak density is greater in LiAlO$_2$, and the distribution is broader in LiGaO$_2$, because of the greater mass of Ga compared with Al. Annealing at temperatures greater than about 350°C causes a reduction in the peak density of ^{2}H in both materials. Note that the implanted profiles do not show diffusion broadening as is seen for doped semiconductors in which hydrogen can attach to donor or acceptor impurities to form stable neutral complexes.[11] It appears that in LiAlO$_2$ and LiGaO$_2$, hydrogen is basically lost from the crystals during thermal annealing, with the remaining hydrogen at each temperature decorating the residual crystal damage (caused by the implantation), This is an issue of potential concern because residual hydrogen in the oxide substrates could be readily transferred to GaN epitaxial films during device processing steps, such as contact alloying, implant activation or implant isolation annealing. However, as seen below, this may be less of an issue than in other potential substrates for GaN epitaxial growth.

Implanted ^{2}H is much less thermally stable in LiAlO$_2$ and LiGaO$_2$ than in sapphire. A wafer of sapphire was implanted with ^{2}H at the same time as the other materials and annealed at the same temperatures as the others. The SIMS profiles for ^{2}H before and after annealing up to 950°C for 10 min are shown in Fig. II.a.2 for sapphire (crystalline Al$_2$O$_3$). No measurable change is caused by such anneals. In Fig. II.a.3, we have plotted the percentage of implanted ^{2}H that remains in LiGaO$_2$, LiAlO$_2$, Al$_2$O$_3$, SiC, GaN, AlN and GaAs after various thermal treatments, based on the data given here and on that reported previously for the nitrides [12,13] and for GaAs.[11] These materials are all potential substrates for III-nitride epitaxy. Clearly the LiAlO$_2$ and LiGaO$_2$ fall at the lower end of the thermal stability range for H retention, which is an advantage because there will be lower levels of residual H after a high temperature growth step. The ^{2}H is presumably in random positions following implantation, and in semiconductors, it moves to regions of strain (defects or impurities) during annealing. The observation that H is not retained at high temperature in the oxide materials is at least an indication that they are free of large densities of defects or impurities, otherwise one would except to observe plateaus forming in the ^{2}H depth profiles at certain annealing temperatures, as for GaAs.[11] It might also be considered that it is better to employ substrates such as alumina and SiC which have extremely high stabilities for hydrogen retention, to prevent diffusion of hydrogen into overlying GaN epilayers. This is a valid viewpoint, although our feeling is that it is better to simply eliminate the hydrogen rather than retain the potential for possible future problems with it.

The fact that ^{2}H is so mobile in LiAlO$_2$ and LiGaO$_2$ at relatively low temperatures is clear from the data in Fig. II.a.4, in which are shown the ^{2}H profiles after exposure to a ^{2}H plasma for 1 h at 250°C. Based on a simple $(4Dt)^{1/2}$ calculation for the diffusion distance, we can estimate diffusivities of $\sim1.1\times10^{-13}$ cm^{-2}s^{-1} in LiAlO$_2$, and $\sim1.7\times10^{-15}$cm^{-2}s^{-1} for LiGaO$_2$. The values are approximately one and three orders of magnitude, respectively, lower than in GaAs at
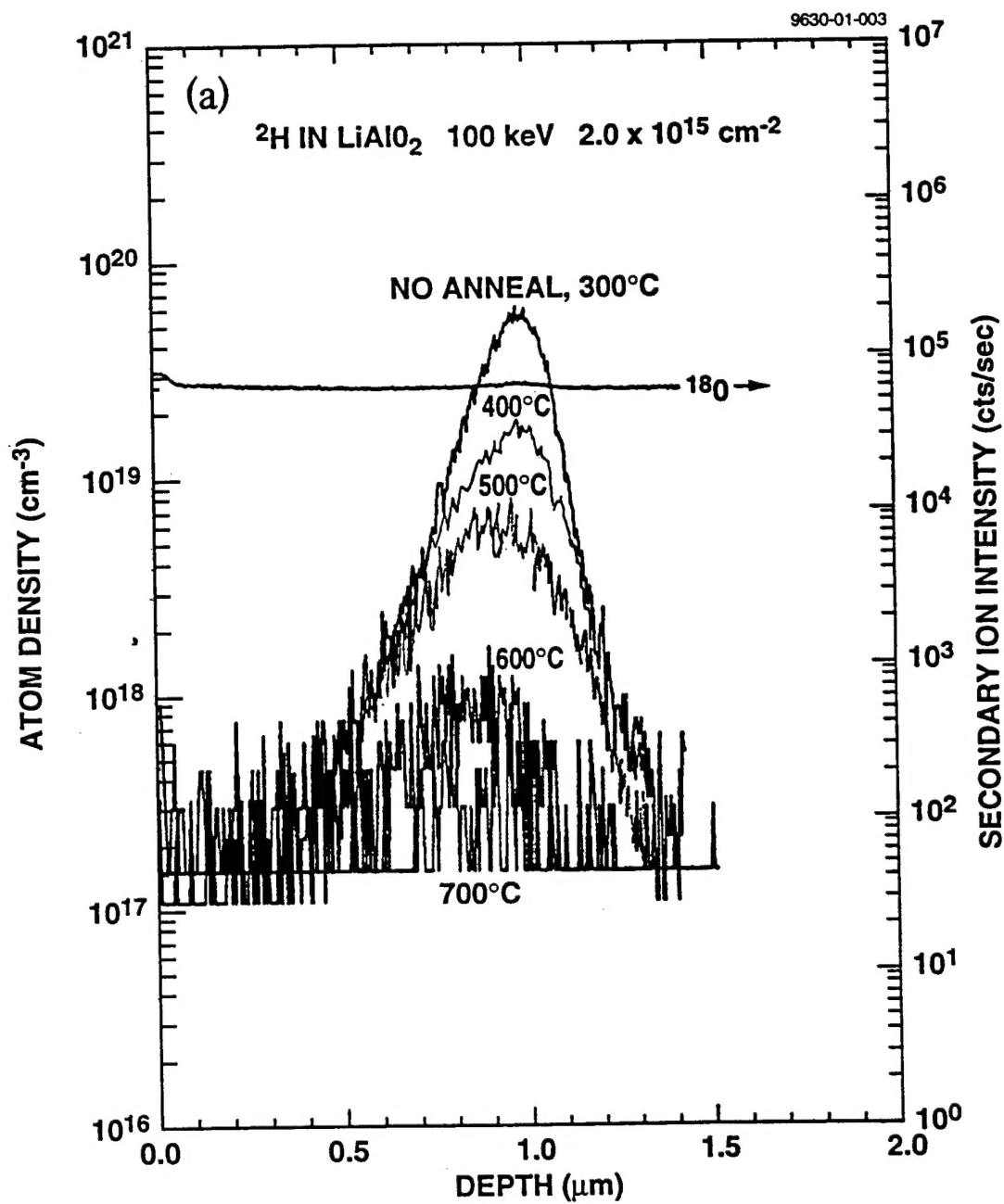
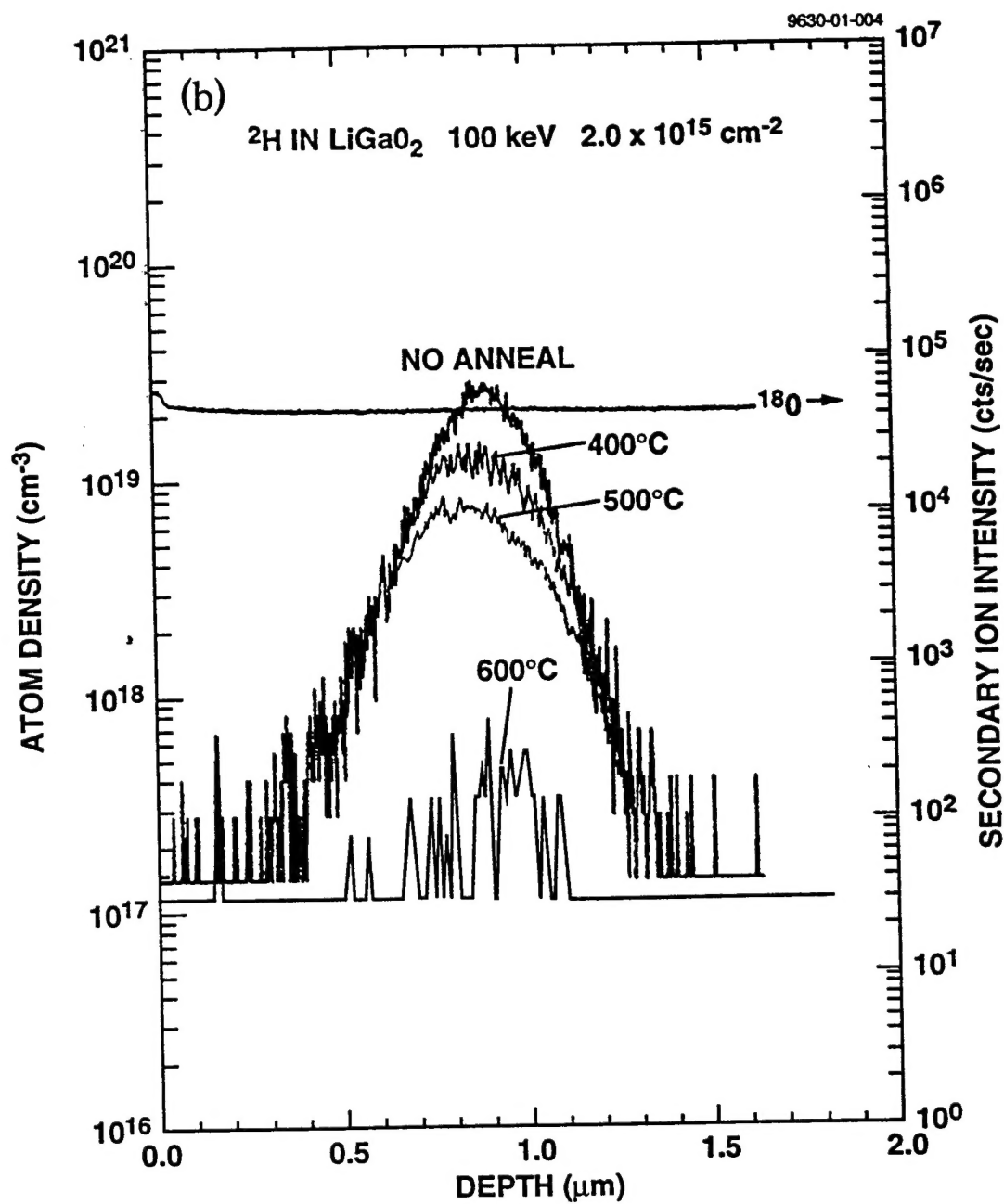Fig. II.a.1a. SIMS profiles of ²H implanted in LiAlO₂ crystals before and after annealing.

9630-01-004

(b)

^{2}H IN LiGaO$_2$ 100 keV 2.0 x 10^{15} cm^{-2}

NO ANNEAL

400°C

500°C

^{18}O →

600°C

Fig. II.a.1b. SIMS profiles of ^{2}H implanted in LiGaO$_2$ crystals before and after annealing.
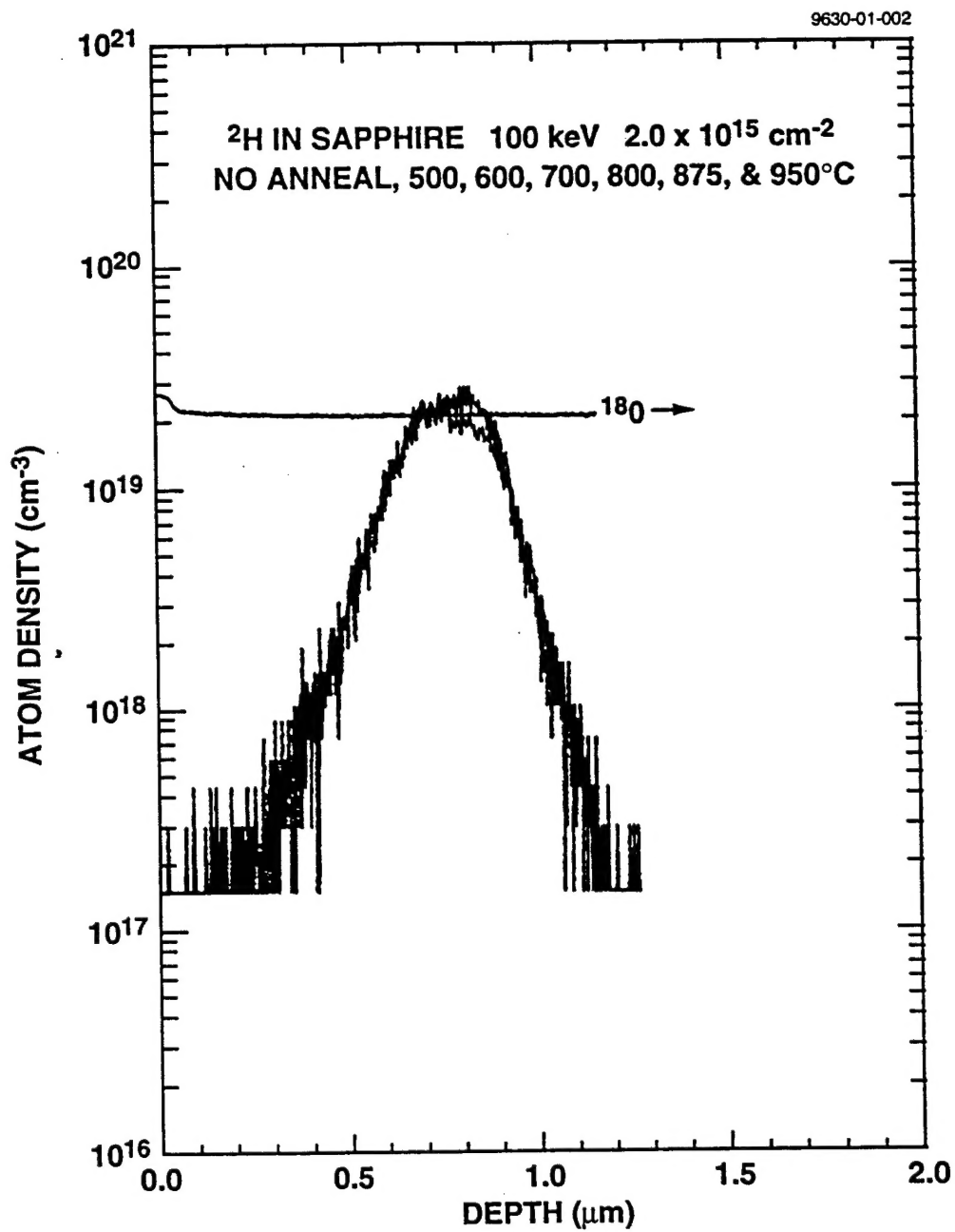
9630-01-002

Fig. II.a.2. SIMS profiles of ^2H implanted in sapphire (Al_2O_3) before and after annealing.
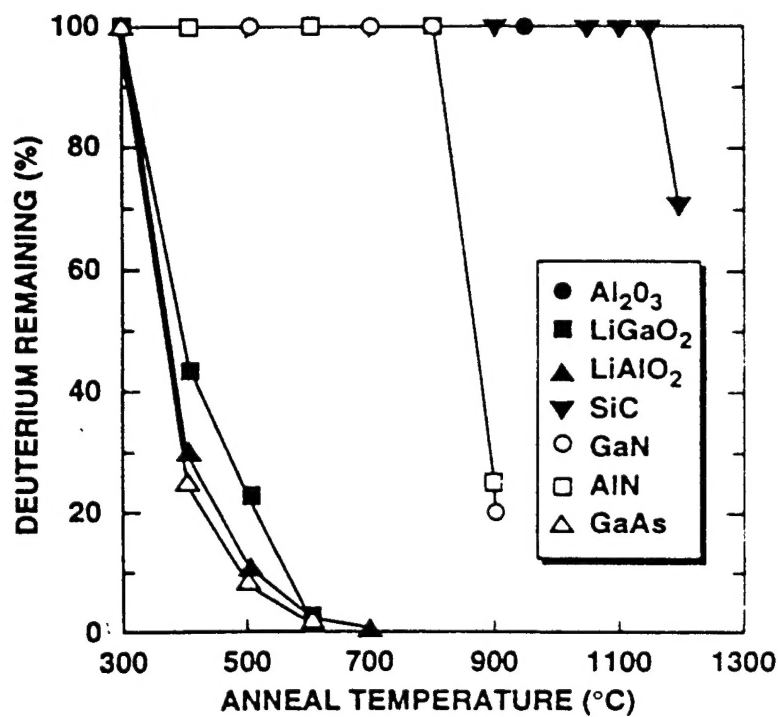
Fig. II.a.3. Percentage of implanted ^{2}H remaining in various crystalline materials after 10 min anneals at various temperatures.
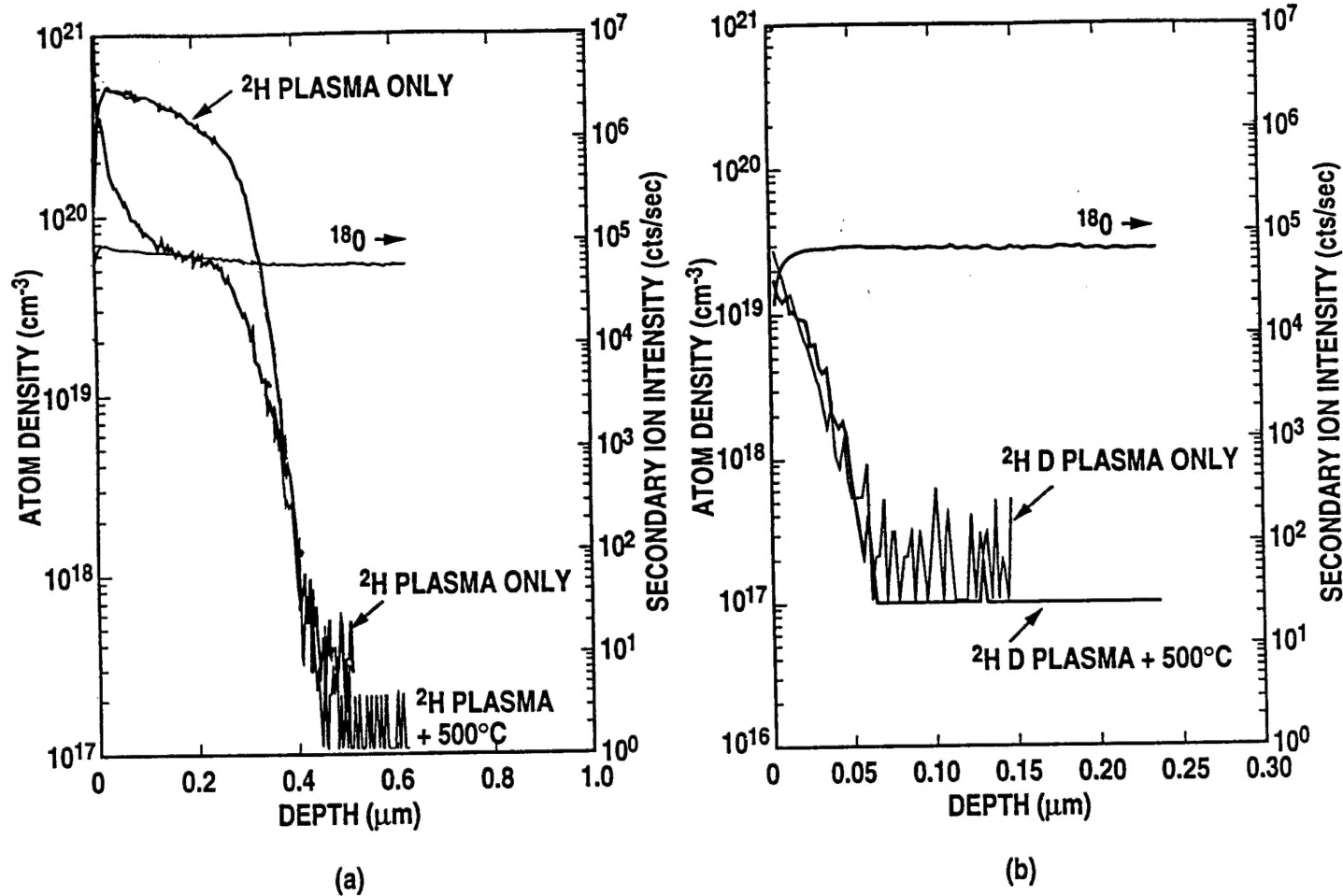
Fig. II.a.4. SIMS profiles of ^{2}H in plasma-exposed LiAlO$_2$ (a) and LiGaO$_2$ (b) crystals, as-treated and after annealing for 1 min at 500°C.

the same temperature.[11] We note that annealing at 500°C again reduces the ^{2}H density in LiAlO$_2$ (whereas there is little change in LiGaO$_2$) without causing significant diffusional broadening of the profiles. The ^{2}H appears to have been lost from the surface. The incorporation depth in LiGaO$_2$ is so shallow that the indiffusion of ^{2}H may be controlled by trapping on defects created by plasma exposure. Clearly however the permeation is significantly slower than in LiAlO$_2$.

In summary, hydrogen is found to diffuse readily in LiAlO$_2$ and LiGaO$_2$ at temperatures as low as 250°C. Outdiffusion begins at less than 400°C, and is complete by 700°C in both materials. The temperatures at which hydrogen is retained are much lower than for SiC, Al$_2$O$_3$, GaN and AlN.

b.   Etching Processes for Fabrication of GaN/InGaN/AlN Microdisk Laser Structures

The group III-nitrides have applications ranging from short wavelength (green, blue, UV) electroluminescent devices for flat panel displays, high definition television and high density compact disks to high temperature electronics.[14-21] To date, little attention has been paid to the development of fabrication processes for these materials. Due to their excellent chemical and thermal stabilities, wet etching has proven difficult. Molten salts can etch GaN at ~400°C, but this is not a practical process. Recently Minsky and Hu[22] reported that laser-enhanced (He-Cd) etch rates of GaN up to a few hundreds of angstrom per minute in 1HCl:10H$_2$O or a few thousand angstroms per minute in 45% KOH:H$_2$O (1:3) were obtained by photo-enhancement of oxidation and reduction reactions occurring in an electrochemical cell.[22] Mileham et al.[23] reported that photoresist developer solutions in which KOH was the active ingredient could etch AlN at rates strongly dependent on the material quality. In terms of dry etching, conventional reactive ion etching at dc biases of ~500V produces GaN rates of $\leq$ 500 Å/min. Most of the plasma chemistries have been based on Cl$_2$. High ion density conditions have been found to produce much higher rates, up to ~0.5 μm/min for Electron Cyclotron Resonance Cl$_2$/H$_2$/CH$_4$/Ar discharges.[24-27]

Both binary (GaN, AlN, InN) and ternary (In$_x$Al$_{1-x}$N, In$_x$Ga$_{1-x}$N) nitrides were grown on Al$_2$O$_3$, GaAs or Si substrates by Metal Organic Molecular Beam Epitaxy, using triethylgallium, trimethylamine alane and trimethylindium as group III precursors and atomic nitrogen from an ECR source (Wavemat).[28] Other samples of AlN prepared by reactive sputtering onto Si substrates were also used for the wet etching studies. These were annealed under N$_2$ in a rapid thermal furnace (Heatpulse 410) face down on GaAs substrates for 10 sec at temperatures from 500-1100°C in order to examine the effect of material quality on etch rate.

Dry etching was performed in a Plasma-Therm SLR 770 ECR system with the samples clamped to a He backside cooled, rf powered (50-250W) chuck. The microwave power was varied from 400-1000W, with the process pressure held constant at 1.5 mTorr. The ICl vapor was injected directly into the ECR source through a mass flow controller, at a total flow rate of 4 standard cubic centimeters per minute. We also added 4 sccm of Ar to enhance the ion-assisted component of the etching.

For wet etching, AZ400K developer solution with ~10% KOH as the active ingredient, was employed at temperatures between 20 and 80°C. Etch rates were determined in all cases by stylus profilometry after removal of the mask material (photoresist, SiN$_x$ or Apiezon wax).

Scanning electron microscopy (SEM) and atomic force microscopy (AFM) were used to examine sidewall undercut and surface smoothness, respectively.

The basic process for forming a microdisk laser in a semiconductor structure is shown schematically in Fig. II.b.1. The whispering gallery lasing modes are generally quenched unless the disk containing the quantum wells or bulk active region is essentially sitting in free space,[29] i.e. a large undercut is needed to form narrow support post. The small active volume requires only small threshold acceptors for lasing, and facets are not required. These devices are readily fabricated in arrays and are possible components of photonic integrated circuits. As seen in Fig. II.b.1 just one mask level and two etch steps are needed — one a non-selective anisotropic pattern transfer and the other a selective undercut of the substrate (or buffer) material. For fabricating nitride-based microdisk lasers,[30] there are several different possible structures. In one version one could employ InGaN quantum wells with GaN cladding layers, grown on a thick AlN buffer. Another possibility involves an Er-doped active region of GaN , AlGaN or AlInN grown on AlN, in which one would seek the enhanced 1.54µm emission reported for GaP(Er) microcavity structures.[31] Er-doped GaN has previously been found to have emission in the blue, green and red portions of the spectrum and thus is promising for catholuminescent field emission display devices.[32]
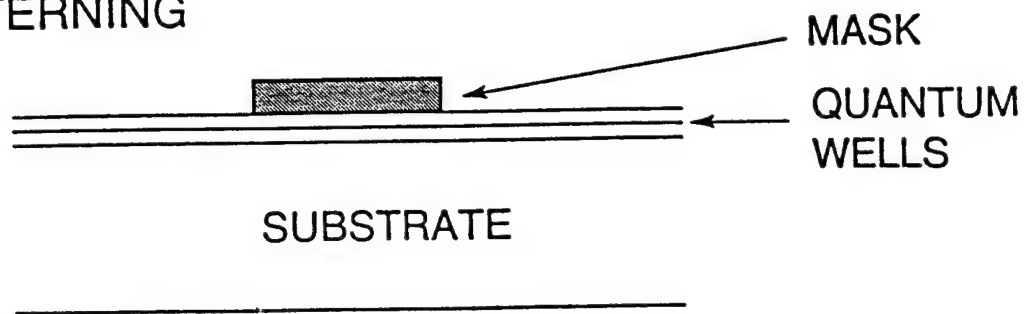
Fig. II.b.2 shows the etch rates of the nitride materials as a function of rf chuck power in 1000 W (microwave) 4ICl/4Ar, 1.5 mTorr discharges. We found the etch rates were almost independent of microwave power above 400W, suggesting the ICl molecule is weakly bound (melting temperature, 27°C) and is easily dissociated into active chlorine and iodine. The etch rates for GaN, InN and InGaN increase rapidly above ~150W rf power, indicating that the etching is desorption limited and that there is much more efficient sputter-assisted removal of the etch products at higher ion energies. The more strongly bonded AlN and InAlN (11.52 eV·atom^{-1} for AlN, 8.92 eV·atom^{-1} for GaN and 7.72 eV·atom^{-1} for InN) have much slower rates than the other materials. We believe etching is limited in these cases by the difficulty in initially breaking the bonds , which must precede etch product formation. The rates achieved for GaN, InN and InGaN are the fastest reported for these materials. The etched surface morphologies were excellent (root-mean square roughness of 2-4 nm over 10x10 µm^2 measured by AFM) over a wide range of plasma conditions. Moreover, at these low rf powers there was no detectable preferential loss of N from GaN as we have observed at higher powers (450W) with Cl$_2$/Ar.

Fig. II.b.3 shows an Arrhenius plot of AlN etch rate in the AZ400K solution as a function of the annealing temperature. The effect of the annealing treatment is to improve the material quality by densifying the film and decreasing the density of defective bonds. For example the UV absorption of thicker films shows n ~75% reduction in midgap states in the sample annealed at 1100°C, relative to the as-deposited material. The wet etching is thermally activated, of the form
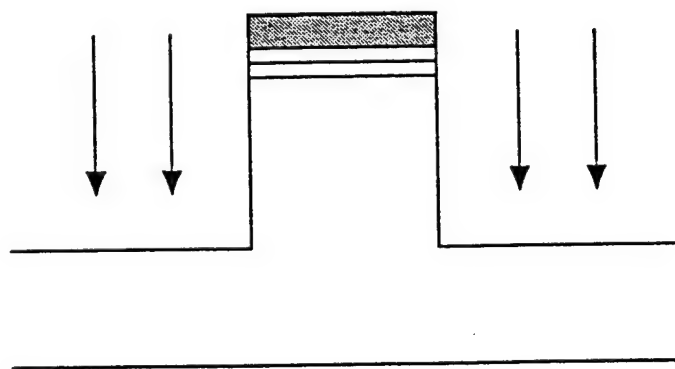
$$R = R_0 exp(-E_a/kT) \quad (1)$$

where R is the etch rate at absolute temperature T, k is Boltzmann's constant, R_0 is a constant which depends on the material quality and E_a is the activation energy for the process. In Fig. II.b.3, the E_a values are all within the range 2.0 ± 0.5 kcal/mol for the AlN, which are typical of

1. PATTERNING

MASK

QUANTUM
WELLS

SUBSTRATE

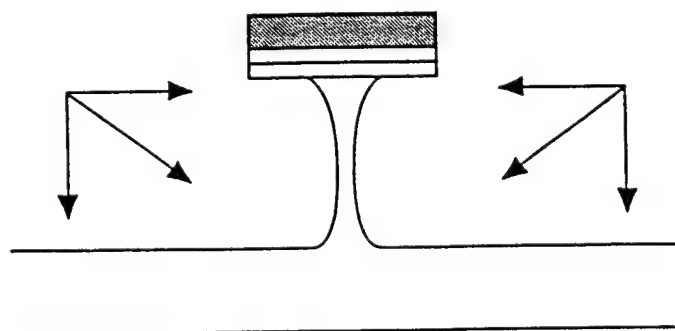## 2. DRY ETCH

3. WET CHEMICAL ETCH

Fig. II.b.1.   Schematic of process for fabrication of a microdisk laser.
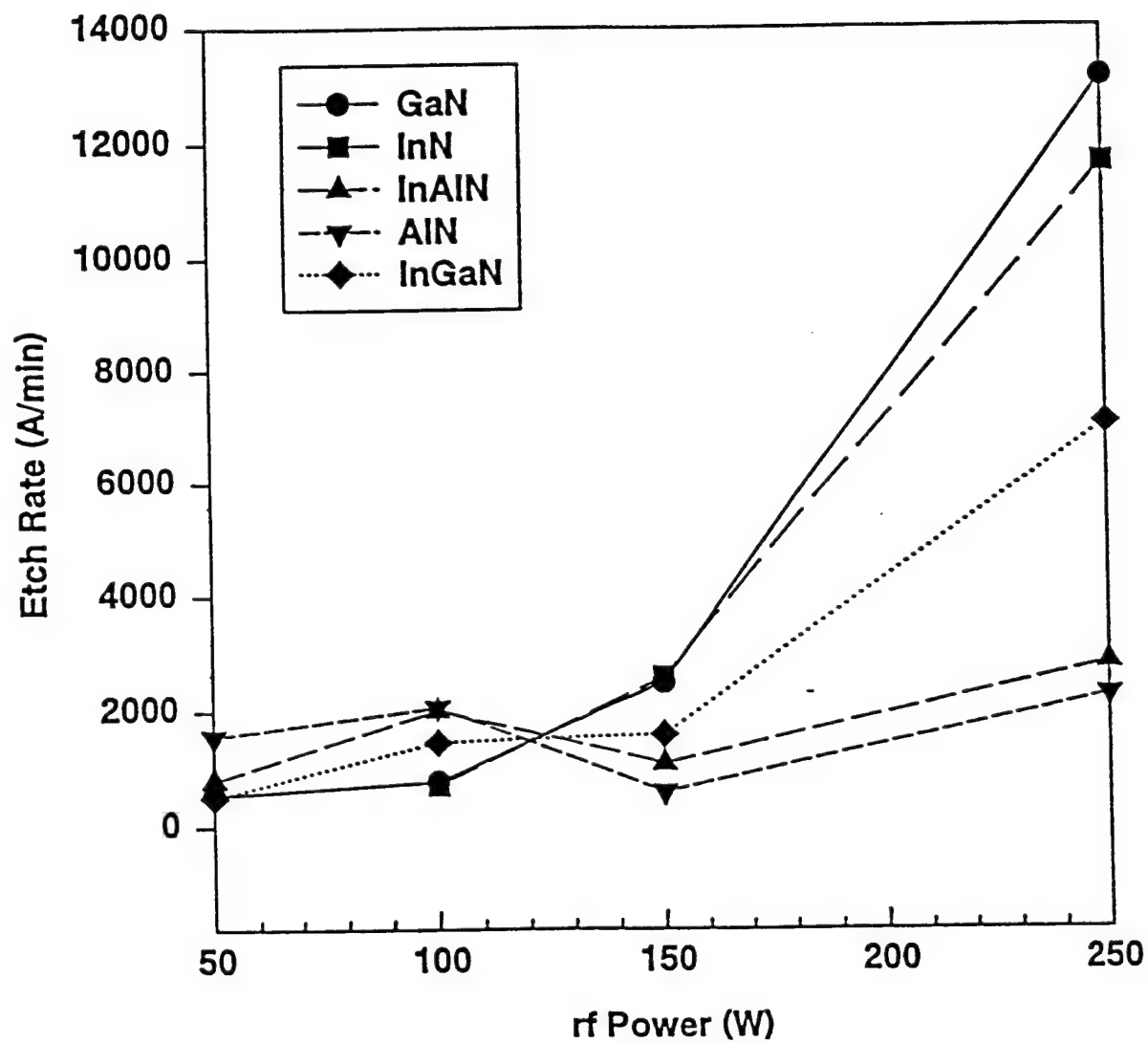
Fig. II.b.2.   Etch rate of III-nitrides as a function of rf power in 4ICl/4Ar, 1000W (microwave), 1.5mTorr discharges.
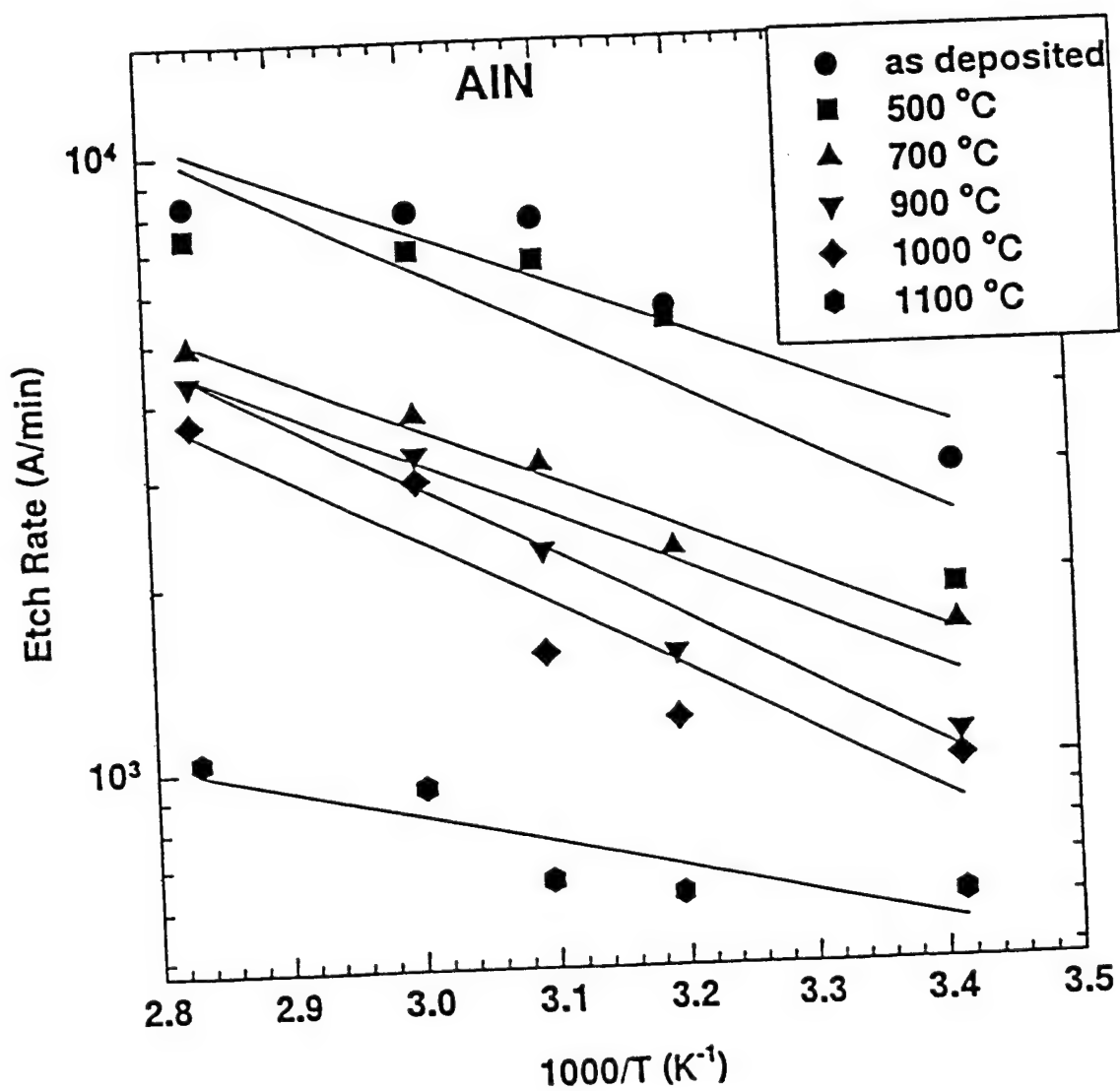
Fig. II.b.3.   Arrhenius plot of AlN etch rates for as-deposited or annealed AlN as a function   of reciprocal etch temperature.

diffusion-limited processes. Much higher activation energies (~15 kcal/mol) were reported for single crystal AlN etched in AZ400K.[10]

The etch rate as a function of temperature for $In_{0.19}Al_{0.81}N$ layers (0.5µm thick) grown on either GaAs or Si substrates is shown in Fig. II.b.4. The material grown on Si is of much poorer quality as measured by x-ray diffraction and absorption measurements (apparently a factor of 3 narrower x-ray peaks and ~50% loss midgap absorption) and this is reflected in the higher etch rates. The data in Figs. II.b.3-4 is convincing evidence that the wet etching in particular is a strong function of material quality, because broken or defective bonds will be more susceptible to attack by the active species in the etch solution.

We measured the composition dependence of $In_xAl_{1-x}N$ etch rate for different solution temperatures. Once again in all cases the activation energies were in the range 2-6 kcal/mol. There was no etching of pure InN (or GaN) in the KOH-based solutions, but we obtained slow etching of $In_xAl_{1-x}N$ even at the x-values of 0.75. The rates in the latter case were approximately an order of magnitude lower than for pure AlN at any temperature.

Using the etching processes developed in this study, we fabricated some microdisk structures in the GaN/InGaN/AlN materials system. The top of Fig. II.b.5 shows SEM micrographs of an array of disks formed by dry etching into the AlN buffer. A subsequent wet etch at 60°C for 10 mins selectively undercuts the AlN, without affecting the GaN/InGaN (lower micrograph in Fig. II.b.5). The roughness on the sidewall of the disks is directly related to the columnar growth mode of the nitrides on Al_2O_3 substrates, and is an issue when considering use of dry etching for formation of waveguides or mirrors where light scattering at rough surfaces must be minimized. Different growth conditions can provide smoother sidewalls, as reported previously.[30]

KOH-based wet etch solutions can be used for selective removal of $In_xGa_{1-x}N$ alloys with In contents as high as 75%.. The rates are a strong function of material quality and are reduced significantly when the samples are annealed, which decreases the density of lattice defects. ICl is an effective plasma chemistry for etching the nitrides — rates in excess of 1 µm/min can be obtained for GaN and InN under ECR conditions.

(III) Ohmic Contacts to p-GaN (Paul Holloway and Jeff Trexler)

Studies continued this quarter emphasizing the contact metallization Cr/Au. The p-GaN:Mg substrates had a carrier concentration of 9.8×10^{16} cm^{-3} and the contacts were deposited by electron beam evaporation with 500Å Cr followed by a 1000Å Au capping layer. The main area of investigation was the interfacial reaction products formed upon a rapid thermal annealing (RTA) treatment at 900°C for 15 seconds in flowing N_2. This heat treatment provided linear current-voltage curves indicative of ohmic contacts with a specific contact resistance $< 4.3 \times 10^{-1}$ Ωcm^2. Transmission electron microscopy (TEM) and X-ray diffraction (XRD) were used to identify the composition of the interfacial reaction products. These results were then compared to previous Auger electron spectroscopy (AES) depth profiles.

Previously, AES depth profiles showed that upon an RTA of 900°C for 15 seconds in the Cr/Au contacts, there was diffusion of Cr through the Au capping layer to the surface and evidence of dissociation of GaN by Cr. A Au:Ga phase has formed just below the surface Cr

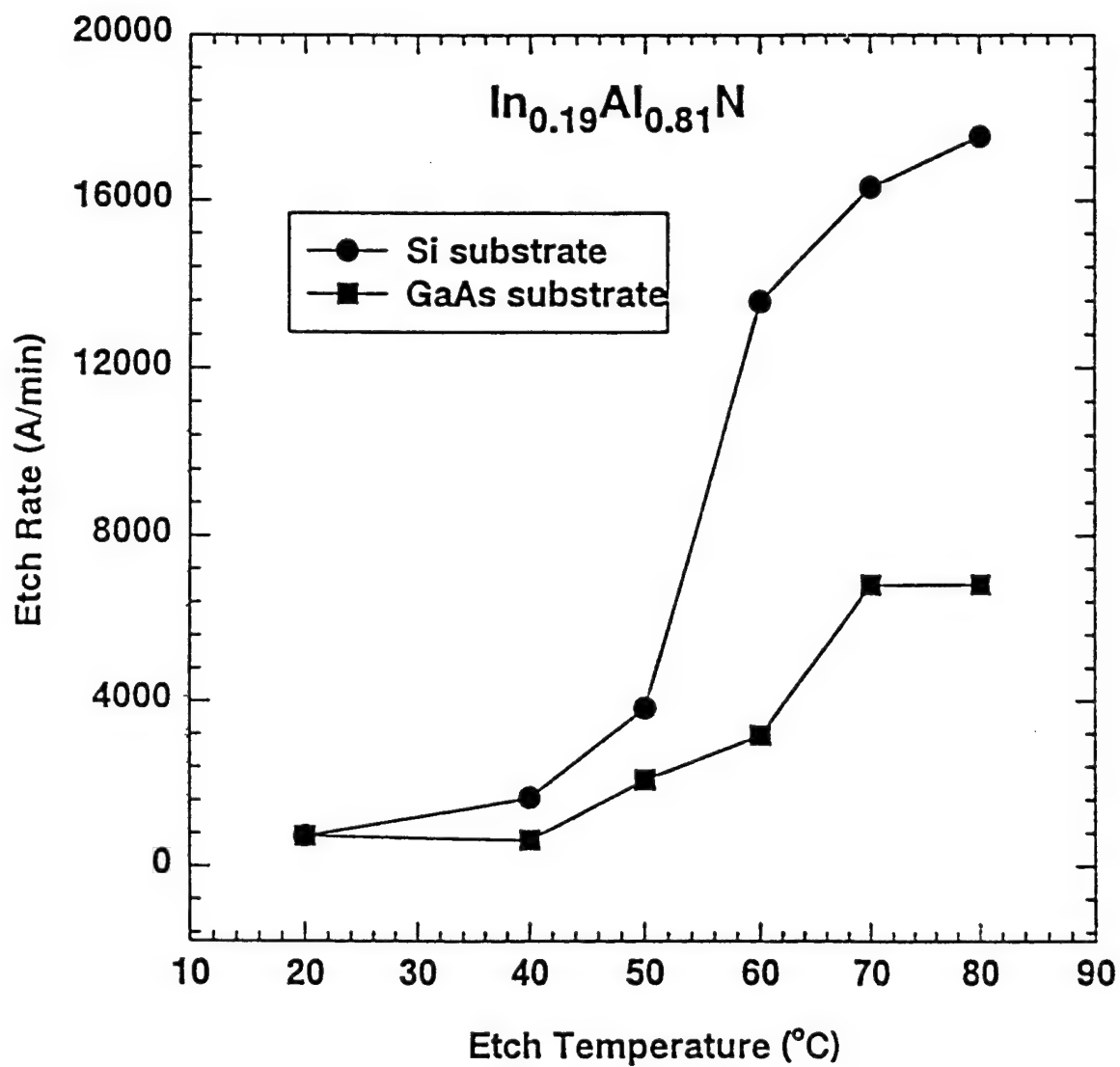**Fig. II.b.4.** Etch rates as a function of temperature for $In_{0.19}Al_{0.81}N$ grown on either Si on GaAs.

Fig. II.b.5. SEM micrographs of (top) an array of microdisks after ECR etching and (bottom) after selective wet etch undercut of the AlN.

layer with the excess N believed to be incorporated into a Cr:N or Cr:GaN phase at the metal/semiconductor interface. It was postulated that this interfacial phase has a higher work function than the individual metals, reducing the potential offset at the interface.

As-deposited TEM micrographs showed a very planar interface between the metal and semiconductor and at the present time sample preparation is being done on an annealed sample to determine the changes in composition. The as-deposited XRD plots showed a large peak from the underlying (002) GaN plane along with evidence of a Au (111) oriented film. No Cr was observed due to the peak overlap of the majority of Cr and Au peaks. This peak was associated with Au due to the larger thickness of the Au layer making it more likely to be detected in XRD. Upon heat treatment there is still a large GaN (002) peak, but the Au (111) peak disappeared. There were many more peaks in this spectrum including peaks associated with the phases GaAu and Cr$_2$GaN. This was very similar to the results provided from the AES depth profiles, but the TEM work will need to be completed to properly assign compositions to these phases.

(IV) Microstructures of Nitridation of the Surface of LiGaO$_2$ (Kevin Jones and Jing Hong Li)

Characterization work of GaN/LiGaO$_2$ was focused on microstructural study on nitridation of the surface of LiGaO$_2$ substrate during last three months. Based on our previous research work, we found that there is disordered region at the surface of the LiGaO$_2$ substrate which may contribute to a high density defects of dislocations and inversion domains in the MOCVD grown GaN films. The surface of LiGaO$_2$ wafers may be damaged during the wafers were made by mechanically cutting, polishing and chemically polishing. It was found that etching the LiGaO$_2$ surface with common inorganic such as HCl degraded the substrate surface quality.[33] The surface microstructure of a substrate is one of very important factors to control the crystalline quality of epitaxy film. It has been shown that atomic rough surface of a substrate leads to formation of some planar defects such as stacking misplacement boundaries (SMBs) and inversion domain boundaries (IDBs).[34] In our previous result, it was shown that there is a amorphous or nano-crystalline interlayer between the grown GaN film and the LiGaO$_2$ substrate.[33] This may be caused by the surface damage of the LiGaO$_2$ by decomposition. Experimental results has shown that nitridation of substrate's surface before completion of epitaxial growth by means of activated nitrogen leads to the reconstruction of its surface and to the improvement of crystalline quality of the growth layer. This method is widely used in molecular-beam epitaxy (MBE) and metal-organic chemical hydride epitaxy for improving growth of nitride films.[35-37] Very little is known about the microstructure of the LiGaO$_2$ and the effect of nidtridation on its surface microstructure. This motivated us to carry out an investigation of the effect of nitridation of the LiGaO$_2$ on its surface microstructure. Here we report our results on the nitridation of the surface measured by high resolution electron microscopy (HRTEM).

Bulk single crystal LiGaO$_2$ was grown by the Czochralski method at Crystal Photonics.[33] The LiGaO$_2$ wafers were made by mechanical cutting, polishing and chemical polishing. The last polishing was a colloidal silica chemo-mechanical polishing to epi-grade

quality of the surface. The nitridation of the $LiGaO_2$ was carried out using ammoina (NH_3). The as-received $LiGaO_2$ was cleaned by acetone and methanol. The $LiGaO_2$ substrates were then inserted into the MOCVD reactor and exposed to a N_2 flow at a temperature between 650 and 900°C for 10 min, followed by a nitridation using NH_3 at different temperatures for 10 min.

Fig. IV.1 shows a cross-sectional HRTEM image of as-received $LiGaO_2$ substrate. It revealed that there was a disordered region at the substrate's surface with a depth of ~10-15 nm. The high contrast in that region indicates that some degree of stress still remain in the disordered region. The bending lattice images were observed, as indicated by arrows, which also indicate that there is some stress remained in the surface region. Below the disordered region, the $LiGaO_2$ show high crystalline quality. Fig. IV.2 shows plan view HRTEM images of (a) as-received $LiGaO_2$ taken along the [001] zone axis, and (b) NH_3-treated $LiGaO_2$ at 650°C for 10 min. Random contrast was observed. Bending of lattice, as indicated by arrows, was also observed. All of these indicate that high strain remained in the $LiGaO_2$, as shown in Fig. IV.2 (a). Selected area diffraction pattern from the NH_3-treated $LiGaO_2$ did not show exist any other phase. It is likely that this phase is too thin to get enough diffraction reflection. But the corresponding HRTEM image show some Moirē fringes, as illustrated by arrows in Fig. IV.2 (b), suggesting that there is another phase overlapped the $LiGaO_2$. Fig. IV.3 shows a cross-sectional HRTEM image of N_2 treated $LiGaO_2$ at 800°C. It revealed that the disordered region observed from the as-received $LiGaO_2$ has disappeared. The surface shows extended terraces with some steps. The steps height is about 5-10 Å. The N_2-treated $LiGaO_2$ also exhibit high degree of crystalline quality. Fig. IV.4 shows a HRTEM image of NH_3-pretreated $LiGaO_2$ at 900°C for 10 min. The surface of the $LiGaO_2$ exhibited again a atomic flat surface structure with steps less than 5 Å. The lattice at the surface was bent with higher contrast compared with the $LiGaO_2$ substrate, indicating either a change of lattice parameters of the $LiGaO_2$ or formation another phase overlapped the $LiGaO_2$.

So far, the most commercialized substrates such as sapphire are far beyond atomically smooth whether after mechanically and chemically polished, and contain some disordered regions at surface and a very high density of surface steps. In the $LiGaO_2$ case, it is possible that the last step of chemical polishing can not remove the damage region caused by mechanical cutting and polishing. This corresponds to an RMS roughness of 3.4 nm.[38] This is confirmed by HRTEM observation that there is a ~10-15 nm deep disordered region at the surface of $LiGaO_2$ as-received. However, after NH_3-treated, results from Auger electron spectroscopy (AES) show that N has been incorporated into the surface of $LiGaO_2$, and that the surface roughness is significantly decreased as the NH_3-treatment temperature is increased, from 0.58 nm at 650°C to 0.1 nm at 900°C.[38] Correspondingly, HRTEM observation reveals that the disordered region observed in the as-received $LiGaO_2$ disappeared in the NH_3-treated $LiGaO_2$. The surface of the NH_3-treated $LiGaO_2$ become atomically flat with smaller steps as the NH_3-treatment temperature increased. This observation is consistent with surface roughness measurement.[38] All of these results show that a big improvement of the surface structure of the $LiGaO_2$ substrate has been achieved by NH_3-treatment.

It has been demonstrated that planar defects such as stacking mismatch boundaries and inversion domain boundaries are mainly caused by the surface steps at the surface of substrates. Nitridation of substrate has been successfully used to reduce surface steps of GaAs using MBE by reconstructing the surface structure and forming a very thin layer of ~1.0 nm GaN where As
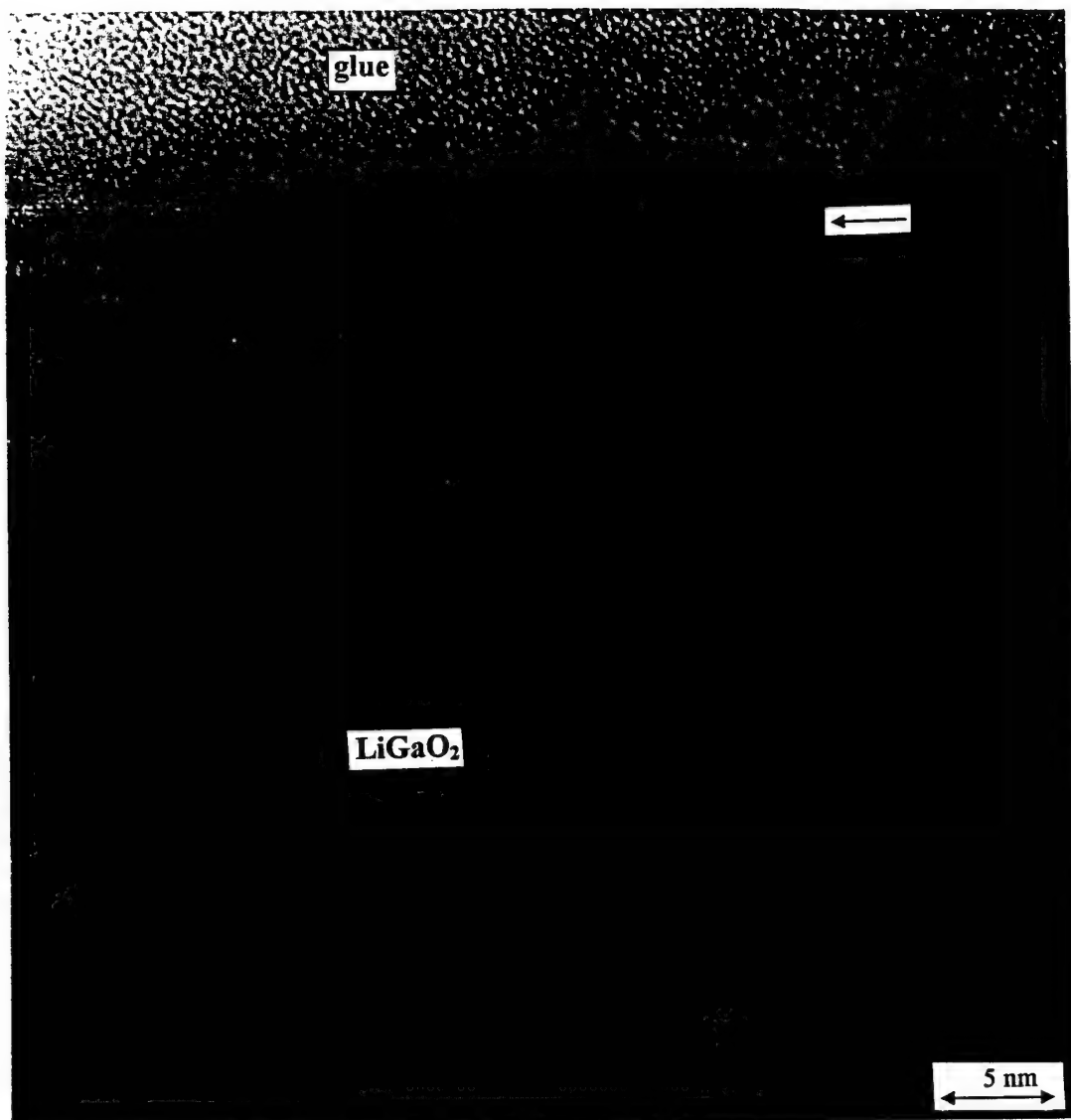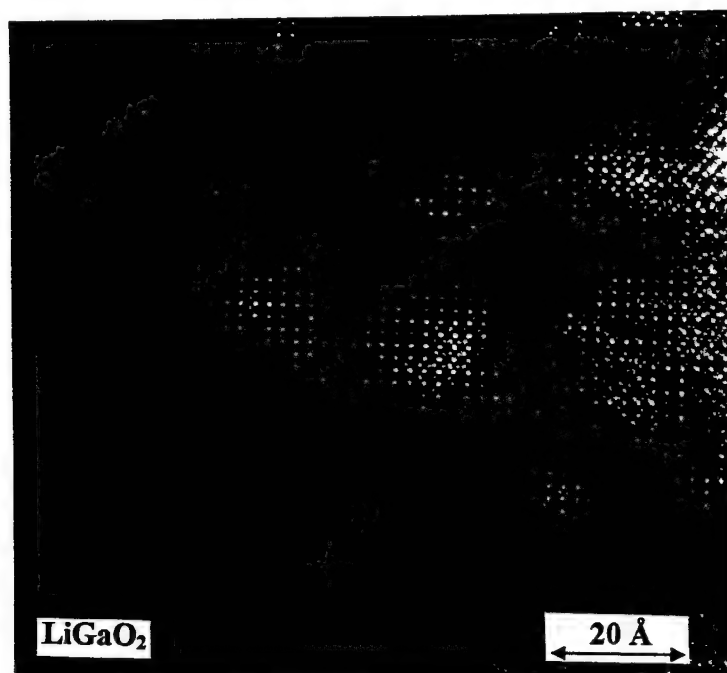
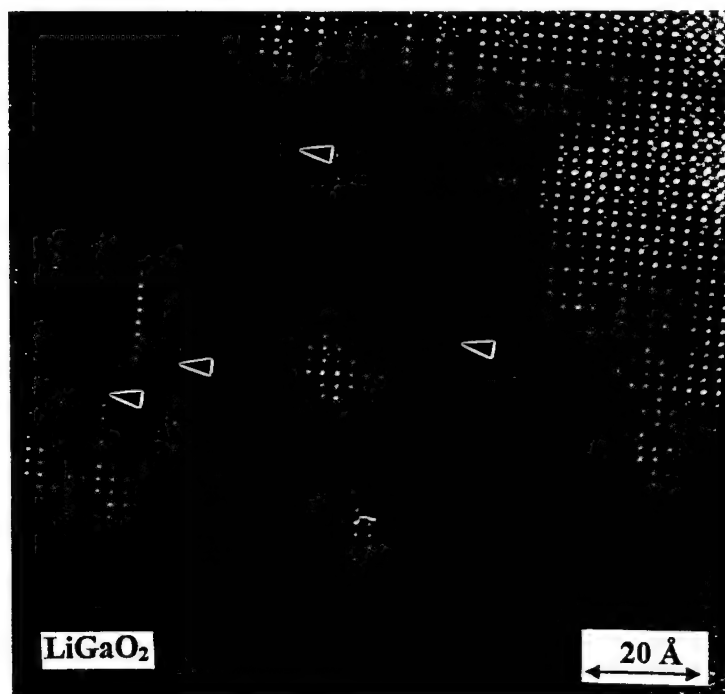**Fig. IV.1.** A cross-sectional HRTEM image of LiGaO$_2$ as-received, showing a disordered region at the surface with a thickness of 10-20 nm

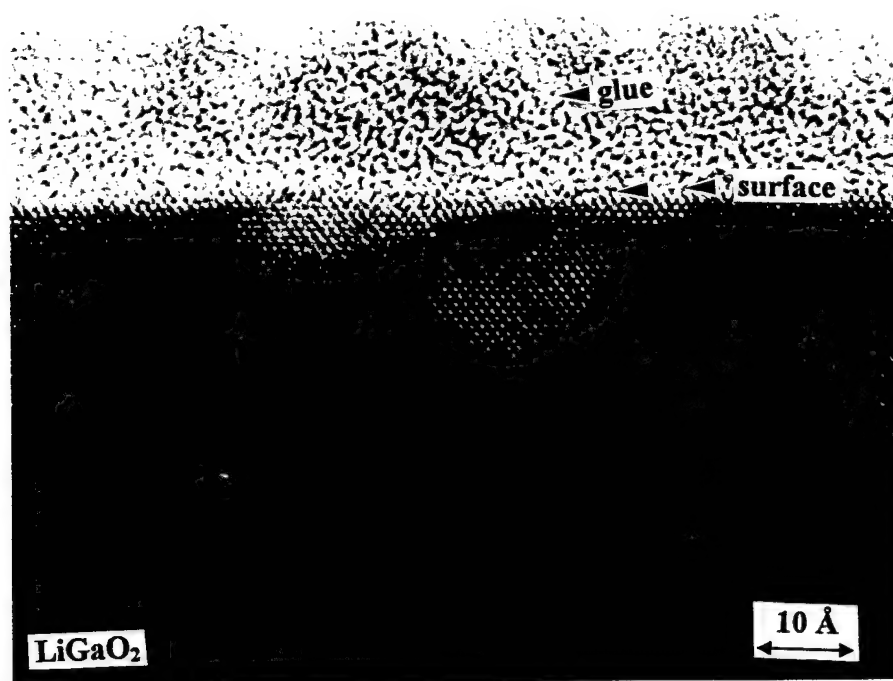Fig. IV.2. Plane view HRTEM images of LiGaO$_2$: (a) as-received and (b) NH$_3$-treated at 900°C for 10 min

Fig. IV.3. A cross-sectional HRTEM image of NH$_3$-treated LiGaO$_2$ at 800°C for 10 min
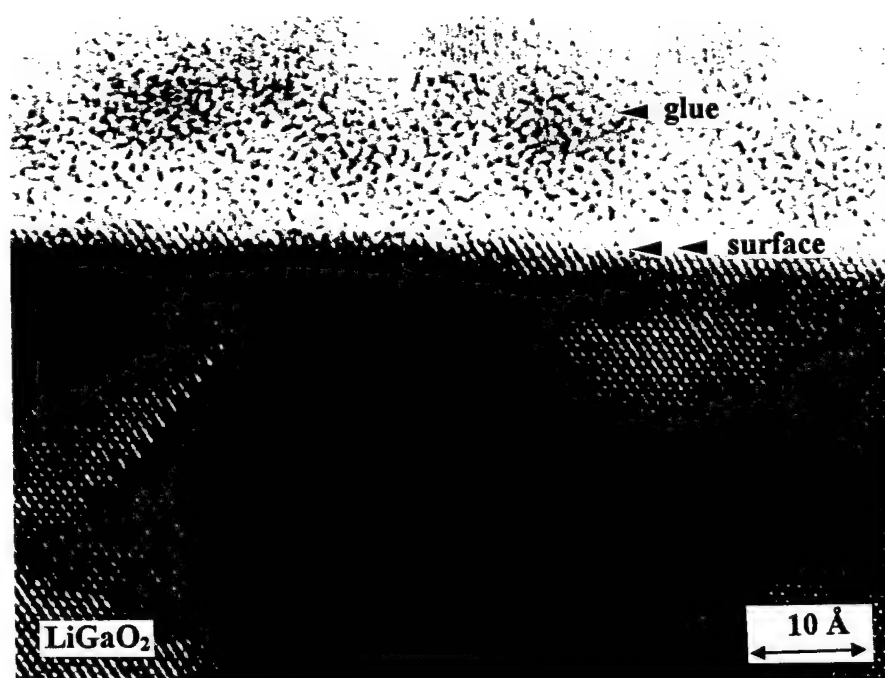

Fig. IV.4. A cross-sectional HRTEM image of LiGaO$_2$ NH$_3$-treated at 900°C for 10 min

atoms are substituted by N atoms.[36,37] Improvement of the NH$_3$-treated LiGaO$_2$ may come either from some chemical reactions at surface region or dissolution of N into the surface of LiGaO$_2$. So far, there is lack of thermodynamic date for the LiGaO$_2$, so it is very difficult to predict what chemical reaction could happen during nitridation of the LiGaO$_2$. Simple thermodynamic calculations shows that GaN is more favorable than LiO$_2$. If the LiGaO$_2$ is terminated with Ga, the N atoms decomposed from NH$_3$ react with the LiGaO$_2$. As a result a thin layer of GaN would form. The structure of LiGaO$_2$ can be derived into a wurtzite structure, so the formation of 1-2 nm GaN film should have the same epitaxial structure with the LiGaO$_2$. But this can not exclude the formation of a mixed Li-Ga-O-N compound at the surface without changing the LiGaO$_2$'s crystal structure. It is also likely that N atoms may interstitially be dissolved into the surface of the LiGaO$_2$ without changing its crystal structure. This may cause the bending of lattice image at the surface of the LiGaO$_2$ because of interstitial dissolve of N atoms by expansion of the lattice of it, as shown in Fig. IV.4. Moreover, the N atoms decomposed from the NH$_3$ could just be absorbed at the surface of the LiGaO$_2$ for a several atomic layers without forming GaN thin film. This makes the LiGaO$_2$ terminated with N, which could contribute to the improvement of GaN growth quality. From our HRTEM results, it is very difficult to see a distinguishable layer at the surface of the LiGaO$_2$ caused by a chemical reaction. Maybe the nitridation time of 10 min is kinetically not long enough to form a GaN thin layer. Cheng etc. have experimentally studied nitridation of the surface of LiGaO$_2$ substrate in molecular-beam epitaxy (MBE) using N$_2$ at 630°C for 3 hours.[39] It was claimed that nitridation of the surface of the LiGaO$_2$ led either to the formation of GaN in the Li-Ga-O matrix or to the formation of about 1.0 nm thin layer of a mixed Li-Ga-O-N compound at the surface. If the LiGaO$_2$ is terminated with Li, lithium hydride could also form. Because LiGaO$_2$ is very sensitive to hydrogen and water,[40] hydrogen from the NH$_3$ or in the environment likely react with the LiGaO$_2$ to form lithium hydride. The mechanism of improvement of the surface of LiGaO$_2$ is not very clear at present. Further work is required. Nevertheless, the nitridation of the surface of LiGaO$_2$ leads to the improvement of the surface of the substrate by using NH$_3$-treatment.

In summary, the surface of LiGaO$_2$ substrate has been nitrided using NH$_3$. Microstructures of surfaces of LiGaO$_2$ as-received and nitridated LiGaO$_2$ have been characterized by HRTEM. Before nitridation, about 10-15 nm deep damage disordered region is found at the surface of LiGaO$_2$ with some steps of ~10 nm at the surface of LiGaO$_2$. The surface of the LiGaO$_2$ is very rough. This may contributed to the formation of inversion domain boundaries and low angle grain boundaries in the MOCVD grown GaN film. After being nitrided by NH$_3$, the surface of LiGaO$_2$ become atomic flat with some small steps of ~1.0 nm, and the roughness of the nitrided LiGaO$_2$ is decreased as the nitridation temperature increases. Nitridation of the LiGaO$_2$ leads to improvement of the surface of the LiGaO$_2$.

(V)   CdZnSe Quntum Well (QW) Diode Laser Material   (Peter Zory)

Our work on the importance of Coulomb Enhancement (CE) in CdZnSe QW lasers will be published in Vol 3001 of the SPIE Proceedings. It was also presented in a talk given by Jeff

Hsu at the Photonics West '97 Conference in San Jose in February. The abstract of the SPIE paper is as follows.

"Data showing the dependence of lasing wavelength on cavity length for CdZnSe single quantum well, buried ridgeguide lasers is presented. The "slope" of the data is opposite in sign to the slope calculated from conventional theory which includes carrier scattering and bandgap renormalization. The calculated slope with Coulomb enhancement included in the model has the correct sign and the correct magnitude to within 30%. Using the Coulomb enhanced model, the key spectral features reported as evidence for an excitonic gain mechanism in room temperature CdZnSe quantum well lasers are reproduced".

Elaborating on the last sentence of the abstract, the key spectral features mentioned are shown in Fig. V.1. The energy E_{ex}, which defines the spectral position of the resonance-like part of the absorption spectrum (the solid curve), is about 17 meV higher than the lasing energy E and about 46 meV lower than the subband gap energy E_{g1}. If CE is not included in the model, the "excitonic peak" does not appear in the absorption spectrum (the solid curve in Fig. V.2). Since E is close to E_{ex} and far from E_{g1}, it is natural to think that the "excitons" represented by the sharp absorption peak are somehow playing a role in determining QW gain. However, since excitons do not exist in the CE-model used and are unlikely to exist in the QW at the carrier densities required for lasing at room temperature, it is probably incorrect to say that the "gain mechanism in CdZnSe lasers is excitonic in nature" (see J. Ding et al, Phys. Rev. Lett., vol 69, pp.1707-1710, 1992). The so-called "excitonic peak, shown in Figure 1, is just due to a collective excitation of the electrons and holes in the QW active layer.

Our work on CE in InGaAs QW lasers, which was used as a guide for the CdZnSe work, has been accepted for publication in the Special Issue of the Journal of Quantum Electronics on Semiconductor Lasers, June, 1997.

InGaN QW LED Material:

Our work on the pulsed electrochemical etching of InGaN QW LED material will be published in Vol. 3002 of the SPIE Proceedings. It was also presented in a talk given by Jason O at the Photonics West '97 Conference in San Jose in February. The abstract of the paper reads as follows.

"A pulsed electrochemical technique for etching MOCVD-grown InGaN/GaN light-emitting diode material at room temperature is reported. The p-GaN and InGaN layers can be etched away in minutes providing access to the n-GaN layer below. Movement of the etch front through the p-n junction region can be observed by monitoring changes in the current pulse shape with time on an oscilloscope".

Fig. V.1. Calculated TE gain/absorption spectra with $N = 4.2 \times 10^{18}$ cm^{-3} (dotted curve) and $N = 6 \times 10^{17}$ cm^{-3} (solid curve) with CS, BGR and CE included. The solid curve has been reduced by a factor of 50.

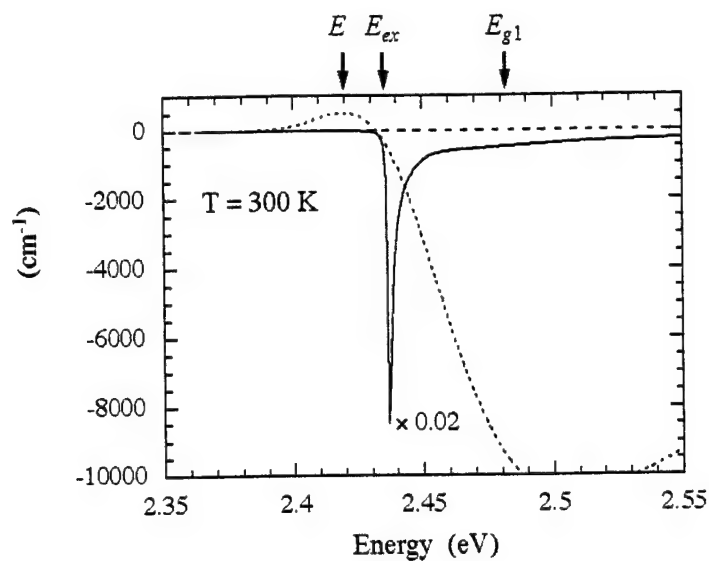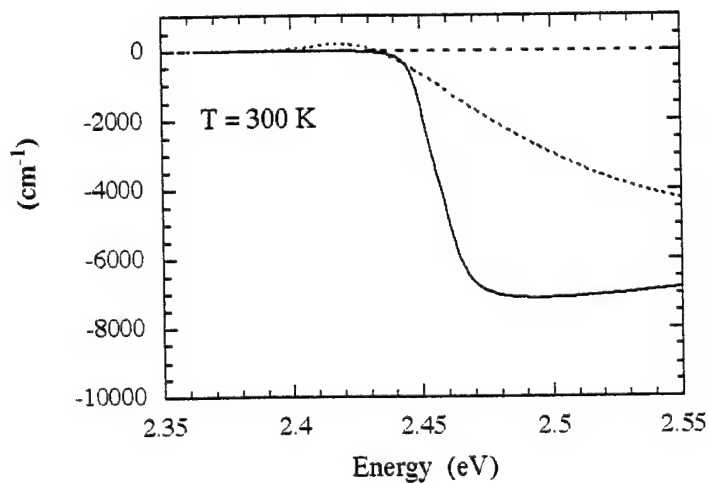**Fig. V.2.** Calculated TE gain/absorption spectra with $N = 4.2 \times 10^{18}$ cm^{-3} (dotted curve) and $N = 6 \times 10^{17}$ cm^{-3} (solid curve) with CS and BGR included and CE ignored.

References:

1. B.L.H.. Chai, Mat. Res. Soc. Symp. Proc. 395, 450 (1996).

2. S. Nakamura, M. Senoh, S. Nagahama, N. Iwasu, T. Yamada, T. Matsushitu, J. Kiyoku and Y. Sugimoto, Jap. J. Appl. Phys. 35, L74 (1996).

3. S. Nakamura, M. Senoh, S. Nagahama, N. Iwasu, T. Yamada, T. Matsushitu, J. Kiyoku and Y. Sugimoto, Jap. J. Appl. Phys. 35, L217 (1996).

4. F.A. Ponce, D.P. Bour, W. Goetz and P.J. Wright, Appl. Phys Lett. 68, 57 (1996).

5. B.N. Sverdlov, G.A. Marlin, H. Morkoc and D.J. Smith, Appl. Phys. Lett. 67, 2063 (1995).

6. H. Liu, A.C. Frenkel, J.G. Kim and R.M. Park, J. Appl. Phys. 74, 6124 (1993).

7. Z. Sitar, M.J. Paisley, B. Yuan, J. Ruan, W.J. Choyke and R.F. Davis, J. Vac. Sci. Technol. B 8, 316 (1990).

8. See for example, S. Strite and H. Morkoc, J. Vac. Sci. Technol. B 10, 1237 (1992).

9. S. Porkowski, presented at 3rd Int. Workshop on Expert Evaluation & Control of Compound Semiconductor Materials and Technologies, Freiburg, Germany, May 1996, to be published in Mat. Sci. Eng. B (1996).

10. J. Schetzina and T.J. Anderson (private communication).

11. J..M. Zavada and R.G. Wilson, Mat. Sci. For. 148/149, 189 (1994).

12. R.G. Wilson, S.J. Pearton, C.R. Abernathy and J.M. Zavada, J. Vac. Sci. Technol. A 13, 719 (1995).

13. J.M. Zavada, R.G. Wilson, C.R. Abernathy and S.J. Pearton, Appl. Phys. Lett. 64, 2724

14. Nakamura, M. Senoh, S. Nagahama, N. Iwasa, T. Yamada, T. Matsushita, H, Kikogu and Y. Sugimoto, Jap. J. Appl. Phys. 35 L74 (1996).

15. C. Wang and R. F. Davis, Appl. Phys.. Lett. 63 990 (1993).

16. M. A. Khan, M. S. Shur and Q. Chen, Electron. Lett. 31 2130 (1995).

17. J.C. Zolper, R.J. Shul, A.G. Baca, R.G. Wilson, S.J. Pearton and R.A. Stall, Appl. Phys. Lett. 68 2273 (1996).

18. Morkoc, S. Strite, G.B. Gao, M.E. Lin, B. Sverdlov and M. Burns, J. Appl. Phys. 76 1363 (1994).

19. D. Walker, X. Zhang, P. Kang, A. Saxler, S. Javadpour, J. Xu and M. Razeghi, Appl. Phys. Lett. 68 2100 (1996).

20. T.J. Schmidt, X.Y. Yang, W. Shan, J.J. Song, A. Salvador, W. Kim, O. Aktas, A. Botchkarev and H. Morkoc, Appl. Phys. Lett. 68 1820 (1996).

21. S. Kurai, Y.Naoi, T. Abe, S. Ohmi andS. Sakai, Jap. J. Appl. Phys. 35 L77 (1996).

22. M. S. Minsky, M. White and E. L. Hu, Appl. Phys. Lett. 68 1531 (1996).

23. J. R. Mileham, S. J. Pearton, C. R. Abernathy, J. D. MacKenzie, R. J. Shul and S. P. Kilcoyne, Appl. Phys. Lett. 67 1119 (1995).

24. L. Zhang, J. Ramer, J. Brown, K. Zhang, L. F. Lester and S. D. Hersee, App. Phys. Lett. 68 367 (1996).

25. I. Adesida, A. T. Ping, C. Youtsey, T. Dow, M. A. Khan, D. T. Olsen and J. N. Kuznia, Appl. Phys. Lett. 65 889 (1994).

26. R. J. Shul, S. P. Kilcoyne, M. Hagerott-Crawford, J. E. Parmeter, C. B. Vartuli, C. R. Abernathy and S. J. Pearton, Appl. Phys. Lett. 66 1761 (1995).

27. S. J. Pearton, C. R. Abernathy and C. B. Vartuli, Electron. Lett. 30 1985 (1994).

28. C. R. Abernathy, Mat. Sci. Eng. Rep. 14 (1995).

References:

1. B.L.H.. Chai, Mat. Res. Soc. Symp. Proc. 395, 450 (1996).
2. S. Nakamura, M. Senoh, S. Nagahama, N. Iwasu, T. Yamada, T. Matsushitu, J. Kiyoku and Y. Sugimoto, Jap. J. Appl. Phys. 35, L74 (1996).
3. S. Nakamura, M. Senoh, S. Nagahama, N. Iwasu, T. Yamada, T. Matsushitu, J. Kiyoku and Y. Sugimoto, Jap. J. Appl. Phys. 35, L217 (1996).
4. F.A. Ponce, D.P. Bour, W. Goetz and P.J. Wright, Appl. Phys Lett. 68, 57 (1996).
5. B.N. Sverdlov, G.A. Marlin, H. Morkoc and D.J. Smith, Appl. Phys. Lett. 67, 2063 (1995).
6. H. Liu, A.C. Frenkel, J.G. Kim and R.M. Park, J. Appl. Phys. 74, 6124 (1993).
7. Z. Sitar, M.J. Paisley, B. Yuan, J. Ruan, W.J. Choyke and R.F. Davis, J. Vac. Sci. Technol. B 8, 316 (1990).
8. See for example, S. Strite and H. Morkoc, J. Vac. Sci. Technol. B 10, 1237 (1992).
9. S. Porkowski, presented at 3rd Int. Workshop on Expert Evaluation & Control of Compound Semiconductor Materials and Technologies, Freiburg, Germany, May 1996, to be published in Mat. Sci. Eng. B (1996).
10. J. Schetzina and T.J. Anderson (private communication).
11. J..M. Zavada and R.G. Wilson, Mat. Sci. For. 148/149, 189 (1994).
12. R.G. Wilson, S.J. Pearton, C.R. Abernathy and J.M. Zavada, J. Vac. Sci. Technol. A 13, 719 (1995).
13. J.M. Zavada, R.G. Wilson, C.R. Abernathy and S.J. Pearton, Appl. Phys. Lett. 64, 2724
14. Nakamura, M. Senoh, S. Nagahama, N. Iwasa, T. Yamada, T. Matsushita, H, Kikogu and Y. Sugimoto, Jap. J. Appl. Phys. 35 L74 (1996).
15. C. Wang and R. F. Davis, Appl. Phys.. Lett. 63 990 (1993).
16. M. A. Khan, M. S. Shur and Q. Chen, Electron. Lett. 31 2130 (1995).
17. J.C. Zolper, R.J. Shul, A.G. Baca, R.G. Wilson, S.J. Pearton and R.A. Stall, Appl. Phys. Lett. 68 2273 (1996).
18. Morkoc, S. Strite, G.B. Gao, M.E. Lin, B. Sverdlov and M. Burns, J. Appl. Phys. 76 1363 (1994).
19. D. Walker, X. Zhang, P. Kang, A. Saxler, S. Javadpour, J. Xu and M. Razeghi, Appl. Phys. Lett. 68 2100 (1996).
20. T.J. Schmidt, X.Y. Yang, W. Shan, J.J. Song, A. Salvador, W. Kim, O. Aktas, A. Botchkarev and H. Morkoc, Appl. Phys. Lett. 68 1820 (1996).
21. S. Kurai, Y.Naoi, T. Abe, S. Ohmi andS. Sakai, Jap. J. Appl. Phys. 35 L77 (1996).
22. M. S. Minsky, M. White and E. L. Hu, Appl. Phys. Lett. 68 1531 (1996).
23. J. R. Mileham, S. J. Pearton, C. R. Abernathy, J. D. MacKenzie, R. J. Shul and S. P. Kilcoyne, Appl. Phys. Lett. 67 1119 (1995).
24. L. Zhang, J. Ramer, J. Brown, K. Zhang, L. F. Lester and S. D. Hersee, App. Phys. Lett. 68 367 (1996).
25. I. Adesida, A. T. Ping, C. Youtsey, T. Dow, M. A. Khan, D. T. Olsen and J. N. Kuznia, Appl. Phys. Lett. 65 889 (1994).
26. R. J. Shul, S. P. Kilcoyne, M. Hagerott-Crawford, J. E. Parmeter, C. B. Vartuli, C. R. Abernathy and S. J. Pearton, Appl. Phys. Lett. 66 1761 (1995).
27. S. J. Pearton, C. R. Abernathy and C. B. Vartuli, Electron. Lett. 30 1985 (1994).
28. C. R. Abernathy, Mat. Sci. Eng. Rep. 14 (1995).

Publications: (Continued)

- C. F. Hsu, P. S. Zory, P. Rees, and M. A. Hasse, "Coulomb enhancement in CdZnSe single quantum well lasers," SPIE Proceedings, vol. 3001, 1997. **(accepted)**.

- C. F. Hsu, P. S. Zory, C. H. Wu and M. A. Emanuel, "Coulomb Enhancement in InGaAs/GaAs Quantum Well Lasers," IEEE J. Selected Topics in Quantum Electronics on Semiconductor Lasers, June, 1997. **(accepted)**.

- J.S. O, P.S.Zory and D.P. Bour, "Pulsed Electrochemical Etching of InGaN/GaN LED material", SPIE Proceedings, vol. 3002, 1997. **(accepted)**.

Presentations:

- "Reactivation of Acceptors and Trapping of H in GaN/InGaN DH," S.J. Pearton, S. Bendi, K.S. Jones, V. Krishnamoorthy, R.G. Wilson, F. Ren, R. Karlicek and R. Stall, 1996 Fall MRS, Boston, December 1996.

- "Cl_2-based Plasma Etching of GaN," R. Shul, S.J. Pearton, C.R. Abernathy, J. Lee and Constantine, 1996 Fall MRS, Boston, December 1996. (Invited)

- "Patterning of $LiGaO_2$ and $LiAlO_2$ by Wet and Dry Etching," J. Lee, S.J. Pearton, C.R. Abernathy, R. Wilson, B. Chen, F. Ren and J. Zavada, 1996 Fall MRS, Boston, December 1996.

- "Plasma Etching of III-Nitrides in ICl/Ar and IBr/Ar Plasma," C. Vartuli, J. Lee, S.J. Pearton, R.J. Shul and C.R. Abernathy, 1996 Fall MRS, Boston, December 1996.

- "Chemical Etching of AlN and InAlN in KOH Solutions," C. Vartuli, J. Lee, J. MacKenzie, S.J. Pearton, C.R. Abernathy, J.C. Zolper, R.J. Shul and F. Ren, 1996 Fall MRS, Boston, December 1996.

- "Photoluminescence, Reflectance and Magnetospectroscopy of Shallow Excitions in GaN," B. Skaromme, B. Goldenberg, J. Long, G. Bulman, C.R. Abernathy and S.J. Pearton, 1996 Fall MRS, Boston, December 1996.

- "Doping Sources for Growth of Group III Nitrides," C.R. Abernathy and T. Groshens, 1996 Fall MRS, Boston, December 1996. (Invited)

- "Ion Implantation and Annealing Studies in III-V Nitrides," J.C. Zolper, S.J. Pearton, J.S. Williams and R.A. Stall, 1996 Fall MRS, Boston, December 1996.

Post Doctoral Associates:
Jing Hong Li with Dr. Jones
Olga Kryliouk with Dr. Anderson

Graduate Students Supported:
George Kim with Dr. Park
Brent Gila with Dr. Park
Jin Hong with Dr. Pearton
K.N. Lee with Dr. Abernathy
Jeff Trexler with Dr. Holloway
Joe Thomes with Dr. Holloway
Todd Dann with Dr. Anderson
Jeff Hsu with Dr. Zory
Jason O with Dr. Zory
Igor Kuskovsky with Dr. Neumark

APPENDIX I

On the kinetics of growth of highly-defective GaN epilayers and the origin of the deep trap responsible for yellow-band luminescence

H. Liu, J. G. Kim, M. H. Ludwig, and R. M. Park

Department of Materials Science and Engineering

University of Florida

Gainesville, FL 32611

Abstract

The kinetics of growth of GaN/(0001) sapphire heteroepitaxial films have been examined in the relatively-low substrate temperature range, 560 to 640°C, using the reflection high energy electron diffraction (RHEED) specular reflection intensity monitoring technique. In particular, an alternate element exposure method of growth was employed in which Ga and N atoms were supplied separately (rather than simultaneously, as in conventional molecular beam epitaxy (MBE)) to the substrate with the inclusion of a time delay between successive Ga flux and N flux exposures. We interpret the observed time dependent recovery of the RHEED specular reflection intensity during the time delay phases to be associated with Ga-N surface molecule migration on Ga-terminated surfaces and the activation energy for this migration process was determined to be 1.45 ± 0.25 eV.

Also, by virtue of comparing the photoluminescence characteristics of epilayers grown by the alternate element exposure method and by conventional MBE and accounting for the presence of a high density of edge-dislocations in our kinetics model, we speculate that the source of the yellow-band luminescence in defective GaN epilayers is electron-hole pair recombination at positively-charged Ga interstitials local to edge-dislocations.

GaN is an attractive material for both short-wavelength optoelectronic device applications and high-power/ high-temperature electronic device applications due to its 3.45eV direct energy gap and its strong interatomic bonding. For instance, exciting progress has recently been reported on the use of GaN-based materials to fabricate short-wavelength diode lasers by Nakamura et al. [1].

However, a persistent problem associated with GaN heteroepitaxial material is the occurrence of the so-called yellow band luminescence centered around 560nm (compared with the 364nm luminescence associated with the GaN band-edge) and the origin of the deep-level-related emission has been the subject of fairly intense speculation [2,3]. The yellow emission band is commonly observed in the photoluminescence (PL) spectra recorded from GaN heteroepitaxial layers grown by various techniques on a variety of lattice - and thermal expansion coefficient - mismatched substrates such as sapphire, SiC and Si [4,5,6]. Typically, GaN heteroepitaxial layers have a high density of dislocations $(10^{10} \sim 10^{11}$ cm^{-2}, for example on sapphire [7]) and it has recently been suggested that the yellow-band luminescence could be associated with the dislocations themselves or perhaps a native point defect that nucleates at the dislocation sites [8]. With regard to native defects in GaN, Neugebauer and Van de Walle [9] have reported that vacancies are more energetically favorable than antisite or interstitial defects according to their first-principles total-energy calculations. However, the calculations were performed assuming thermodynamic equilibrium and without consideration of a high density of dislocations. Since GaN heteroepitaxial layers exhibit a high dislocation density, it seems highly likely that such structural defects will play a significant role in influencing the kinetics of epitaxial growth and in controlling point defect generation.

The kinetics of growth in the case of highly defective GaN epilayers were of concern in the work reported in this letter, particularly with regard to adsorption and migration processes occurring in the presence of dislocations terminating at the free-surface.

In order to study the growth kinetics, surface morphological changes were monitored in-situ and in real-time during crystal growth of GaN epilayers on (0001) sapphire substrates by observing the RHEED (reflection high-energy electron diffraction)

2

specular reflection intensity as a function of time during source shuttering operations. The GaN epilayers were grown using a modified migration enhanced epitaxy (MEE) approach which is itself a variant of molecular beam epitaxy (MBE). The modified MEE approach involved exposing the substrate to Ga and N fluxes separately (rather than simultaneously as in conventional MBE) in an alternate element exposure fashion with the inclusion of a time delay between closing the Ga source shutter and opening the N source shutter during each cycle. This time delay was designed to promote even more extensive migration than would be possible employing conventional migration enhanced epitaxy. The alternate element exposure method is feasible in the case of GaN growth on c-plane sapphire since in the c-axis direction(direction normal to the c-plane), the GaN crystal is comprised of alternate layers of Ga and N atoms.

GaN epilayers were grown on c-plane sapphire substrates in an MBE chamber employing a conventional effusion source for Ga and an rf plasma discharge source (manufactured by Oxford Applied Research Ltd.) designed to provide a flux of reactive N atoms [10]. We have previously reported the growth of GaN epilayers using the OAR radical source [11,12].

C-plane sapphire substrates (cut 0.2° off (0001)) obtained from Union Carbide were employed. Ex-situ substrate preparation consisted of successive rinses in trichloroethane, acetone and methanol followed by etching in H_2SO_4 : H_3PO_4 (3:1) at 160°C for 15 minutes. The substrates were then heat-treated in the MBE growth chamber for 60 minutes at 750°C which yielded a well developed streaky RHEED pattern. Following cleaning, the sapphire substrates were then nitrided by exposure to the flux from the reactive atom source at the same 750°C temperature for about 20 minutes at which point a RHEED pattern indicative of an AlN surface layer was observed.

Following nitridation, the substrate temperature was lowered to 500°C whereupon a 300Å thick GaN buffer layer was grown by simultaneously exposing the substrate to Ga and N fluxes, i.e., a buffer layer was grown by conventional MBE. The Ga and N source shutters were then closed and the substrate temperature was raised to be in the range, 560 to 640°C, for the modified MEE growth experiments presently reported.

3

GaN epilayers were grown on the low temperature buffer layers by employing a source shutter sequencing program, one cycle of which resulted in the following: a 10sec. N flux exposure, followed by a 5sec. Ga flux exposure, followed by a time delay prior to the next N flux exposure. The time delay (time allowed to elapse between closing the Ga source shutter and opening the N source shutter) was selected based on our RHEED specular reflection intensity observations (see below). The GaN epilayers were grown to a thickness of 3,300Å and were characterized ex-situ using PL analysis in which the samples were excited by the 325nm wavelength output of a HeCd laser providing a power density of 30 mWmm^{-2} on the sample. The luminescence signal was dispersed by a 0.3 m single-grating monochromator and detected by a photomultiplier tube.

The RHEED specular reflection intensity (with the electron beam probing in the [1$\bar{2}$10]) was monitored during the exposure and time delay phases using a CCD camera-based monitoring system. As discussed in the literature [13], the intensity of the RHEED specular reflection provides a relative measure of the degree of surface roughness; the smoothest surface yields the most intense specular reflection while the roughest surface on the atomic level yields the lowest intensity. A specular reflection having a temporal variation, therefore, is indicative of a varying surface morphology during crystal growth, typically as a consequence of time-dependent kinetic processes.

As mentioned above, the substrate was alternately exposed to an N flux (for 10 sec.) and a Ga flux (for 5 sec.) with a time delay inserted between the Ga and N flux exposures and a typical specular reflection intensity trace recorded is as shown in Fig. 1 which repeated itself during each growth cycle. As can be seen from the figure, the intensity of the specular reflection was a strong function of the status of the surface in terms of the species present and the particular kinetic processes taking place. Our interpretation of these observations is discussed below in the growth model discussion.

The trace shown in Fig. 1 was recorded from a film grown at 600°C. Similar specular reflection intensity traces were observed during growth at a variety of substrate temperatures over the temperature range, 560 to 640°C. In all cases the traces displayed cyclic behavior in response to the source shutter sequencing employed. However, the specific nature of the trace recorded during the time delay phase was substrate

temperature dependent. Specifically, the time to reach maximum reflection intensity following closure of the Ga source shutter was substrate temperature dependent as was the magnitude of the maximum in the specular reflection. In the case of a substrate temperature of 600°C, for instance, the maximum in the specular reflection intensity was reached after a 30 sec. time delay (see Fig. 1). Shorter recovery times were observed for substrate temperatures higher than 600°C while longer recovery times were noted at lower substrate temperatures.

Recovery times (times to reach maximum specular reflection intensity) following closure of the Ga source shutter are plotted in Fig. 2 versus reciprocal substrate temperature. If it is assumed that these data are indicative of a kinetic process, the activation energy of the process would be 1.45 ± 0.25 eV. We speculate that 1.45 ± 0.25 eV represents the activation energy for Ga-N molecule migration on a Ga-terminated surface in the absence of an N flux (see growth model discussion below).

As mentioned above, the intensity of the recovered specular reflection signal was found to be substrate temperature dependent. In fact, a substrate temperature of 600°C was found to yield the most intense (maximum) specular reflection signal. Also, as indicated in Fig. 1, a 30 sec. time delay was required to obtain maximum signal recovery during each cycle for a substrate temperature of 600°C. Consequently, a GaN epilayer was grown for analysis at 600°C under the following alternate element exposure conditions for each cycle: a 10sec. N flux exposure, followed by a 5sec. Ga flux exposure, followed by a 30sec. time delay following closure of the Ga shutter prior to opening the N shutter. A total of 2,000 cycles were employed which yielded a GaN epilayer thickness of 3,300Å, implying a 0.63 GaN monolayer per cycle growth rate. A 3,300Å thick GaN epilayer was also grown by conventional MBE (i.e., with both Ga and N fluxes arriving at the substrate simultaneously) at a substrate temperature of 600°C for comparison purposes.

Room temperature PL analysis was performed on both GaN epilayers and the spectra recorded are shown in Fig. 3. As can be seen from the figure, the spectra are markedly different. In the case of the MBE-grown film, a significant yellow-band emission is present together with a rather weak band-edge emission, whereas only a strong

band-edge emission is evident in the case of the film grown using the precise alternate element exposure method outlined above. Consequently, it appears that the luminescence characteristics of GaN epilayers are directly related to the promotion (or lack thereof) of critical migration processes.

We have made an attempt to understand the growth kinetics associated with our alternate element exposure mode of growth by interpreting the status of the surface at critical points on the specular reflection intensity trace recorded during each growth cycle. The critical points are illustrated in Fig. 1 and correspond to the following: (a) surface following Ga flux exposure and time delay prior to N flux exposure, (b) surface following a 10sec. N flux exposure, (c) surface following a 5sec. Ga flux exposure, (d) surface following a 15sec. time delay after the Ga flux exposure and, (e) surface following a 30sec. time delay after the Ga flux exposure. It should be noted that these critical times correspond to a substrate temperature of 600°C. It should also be noted that for the particular Ga flux level employed we estimate that a 5 sec. Ga flux exposure would result in the supply of a just sufficient Ga atom population with regard to the N surface atom coverage during each cycle. Consequently, we have not considered desorption of excess Ga to be a significant factor in terms of the recovery of the RHEED specular reflection intensity signal during the time delay phases. The corresponding surfaces in terms of the arrangement of atoms at each of these critical points in time are illustrated in Fig. 4.

If we first ignore the presence of terminating edge-dislocations, at point (a) in Fig. 1 the surface is Ga-terminated and is expected to be a relatively-stable surface since each surface Ga atom shares all three of its valence electrons with three underlying N atoms, i.e., there will be no dangling bonds perpendicular to the surface in this case (surface (a), Fig. 4). Since the 3 valence electrons associated with each surface Ga atom participate in bonds with underlying N atoms, a dipole will exist at each Ga site with the positive end of the dipole appearing on the surface side at each Ga atom site. Incoming N atoms during the N-flux exposure will be polarized by the surface charge and it is expected that the N atoms will associate with surface Ga atoms via weak Van der Waals bonds (surface (b), Fig. 4). The minimum in the specular reflection intensity occurring during the N flux exposure, we believe, corresponds to 50% coverage of N atoms on the surface (see Fig.

1). Upon subsequent Ga flux exposure, the in-coming Ga atoms will react with the available N surface atoms to form Ga-N molecules (surface (c), Fig. 4) and, again, the behavior of the specular reflection intensity during the Ga flux exposure reflects the fractional surface coverage changes. During the time delay phase, i.e., when no further Ga or N atoms are arriving, we expect the Ga-N surface molecules which are only weakly bonded to the surface to migrate on the Ga-terminated surface to step edges causing an increase in the specular reflection intensity (surface (d), Fig. 4). When a maximum has been reached in the specular reflection intensity, we believe that all of the migrating Ga-N molecules will have been incorporated and the surface will again be Ga-terminated (surface (e), Fig. 4), however, as suggested in Fig. 4, a complete monolayer of GaN has not been grown during one cycle. In fact, as mentioned above, the GaN epilayer growth rate was determined to be ~ 0.63 monolayer/cycle for the alternate element exposure method employed. Hence, the step front moves about 63% of a terrace length per cycle.

Our GaN surfaces, however, are non-ideal due to the presence of a high density of edge-dislocations which terminate at the free-surface. If we assume that we have around 10^{10} cm^{-2} dislocations and that the substrate is cut-off the (0001) plane by 0.2°, there will be at least one dislocation on each terrace. Consequently, our model also has to consider the influence of these dislocations on the growth kinetics.

As indicated in Fig. 4, when edge-dislocations are present on a Ga-terminated surface (surface(a), Fig. 4), there will be one unsatisfied electron per dislocation. Consequently, since N atoms are strongly electronegative, in-coming N atoms, during the N flux exposure, are likely to accept the available electrons at the dislocation sites thus forming partially-ionic bonds. Since additional space is available at the dislocation site, we speculate that during a subsequent Ga flux exposure two Ga atoms can interact with each of the N atoms at the dislocation sites. We speculate that during the subsequent time delay phase, the extra Ga atoms have sufficient time to migrate and combine with available N atoms or be desorbed from the surface.

In contrast, such time delays are not provided during conventional MBE-growth of GaN and we speculate that the extra Ga atoms can become trapped at dislocation sites as interstitial defects in MBE grown material.

In summary, since the yellow-band luminescence is significant in the PL spectra recorded from MBE-grown GaN epilayers but is absent in the spectra from material grown by our alternate element exposure method (see Fig. 3), we speculate that the source of the yellow-band luminescence is electron-hole pair recombination at positively-charged Ga interstitials local to dislocations. It is intriguing to note that Ponce et al. [8] have shown experimentally that the spatial distribution of the yellow-band luminescence in GaN epilayers correlates well with the spatial distribution of the dislocations in the material, which strongly supports our postulate concerning the origin of the deep level defects.

References

1. S. Nakamura, M. Senoh, S. Nagahama, N. Iwasa, T. Yamada, T. Matsushita, H. Kiyoku, and Y. Sugimoto, Jpn. J. Appl. Phys., 35, L74 (1996).

2. W. Götz, N.M. Johnson, R.A. Street, H. Amano, and I. Akasaki, Appl. Phys. Lett. 66, 1340 (1995).

3. R. Singh, R.J. Molnar, M.S. Ünlü, and T.D. Moustakas, Appl. Phys. Lett. 64, 336 (1994).

4. A. Ohtani, K.S. Stevens, and R. Beresford, Appl. Phys. Lett. 65, 61 (1994).

5. T. Sasaki and T. Matsuoka, J. Appl. Phys. 77, 192 (1994).

6. P. Kung, X. Zhang, D. Walker, A. Saxler, J. Piotrowski, A. Rogalski, and M. Razeghi, Appl. Phys. Lett. 67, 3792 (1995).

7. S.D. Lester, F.A. Ponce, M.G. Craford, and D.A. Steigerwald, Appl. Phys. Lett. 66, 1249 (1995).

8. F.A. Ponce, D.P. Bour, W. Götz, and P.J. Wright, Appl, Phys. Lett. 68, 57 (1996).

9. J. Neugebauer and C.G. Van de Walle, Phys. Rev. B, 50, 8067 (1994).

10. R.M. Park, J. Vac. Sci. Techol. A 10, 701 (1992) ; R.P. Vaudo, Z. Yu, J.W. Cooke Jr., J.F. Schetzina, Opt. Lett. 18, 1843 (1993).

11. H. Liu, A.C. Frenkel, J.G. Kim, and R.M. Park, J. Appl. Phys. 74, 6124 (1993).

12. J.G. Kim, A.C. Frenkel, H. Liu, and R.M. Park, Appl. Phys. Lett. 65, 91 (1994).

13. J.H. Neave, B.A. Joyce, P.J. Dobson, and N. Norton, Appl. Phys. A 31, 1 (1983).

Figure Captions

Fig. 1 A typical RHEED specular reflection intensity trace recorded during one cycle of the alternate element exposure mode of growth comprising a 10 sec. N flux exposure, a 5 sec. Ga flux exposure and a time delay prior to a subsequent N flux exposure. The trace was recorded at a substrate temperature of 600°C. The critical points in time labeled, (a) - (e), are discussed in the text with reference to Fig. 4.

Fig. 2 RHEED specular reflection recovery time (time to reach maximum signal intensity) after closing the Ga source shutter (prior to opening the N source shutter) plotted versus reciprocal substrate temperature.

Fig. 3 Room temperature photoluminescence spectra recorded from (a), a GaN film grown by conventional MBE and (b), a film grown using the alternate element exposure method. Both films were grown at a substrate temperature of 600°C.

Fig. 4 GaN heteroepitaxial growth kinetics model for one cycle of the alternate element exposure method of growth. Illustrations, (a) - (e), represent the status of the surface at the points in time shown on the RHEED specular reflection intensity trace of Fig. 1 labeled, (a) - (e), respectively. Also shown is the speculated impact of a terminating edge-dislocation which effectively traps an extra Ga atom that is subsequently released during the time delay phase (see Fig. 1).

N shutter open
for 10 sec.

Time-delay

N shutter closed

Ga shutter open
for 5 sec.

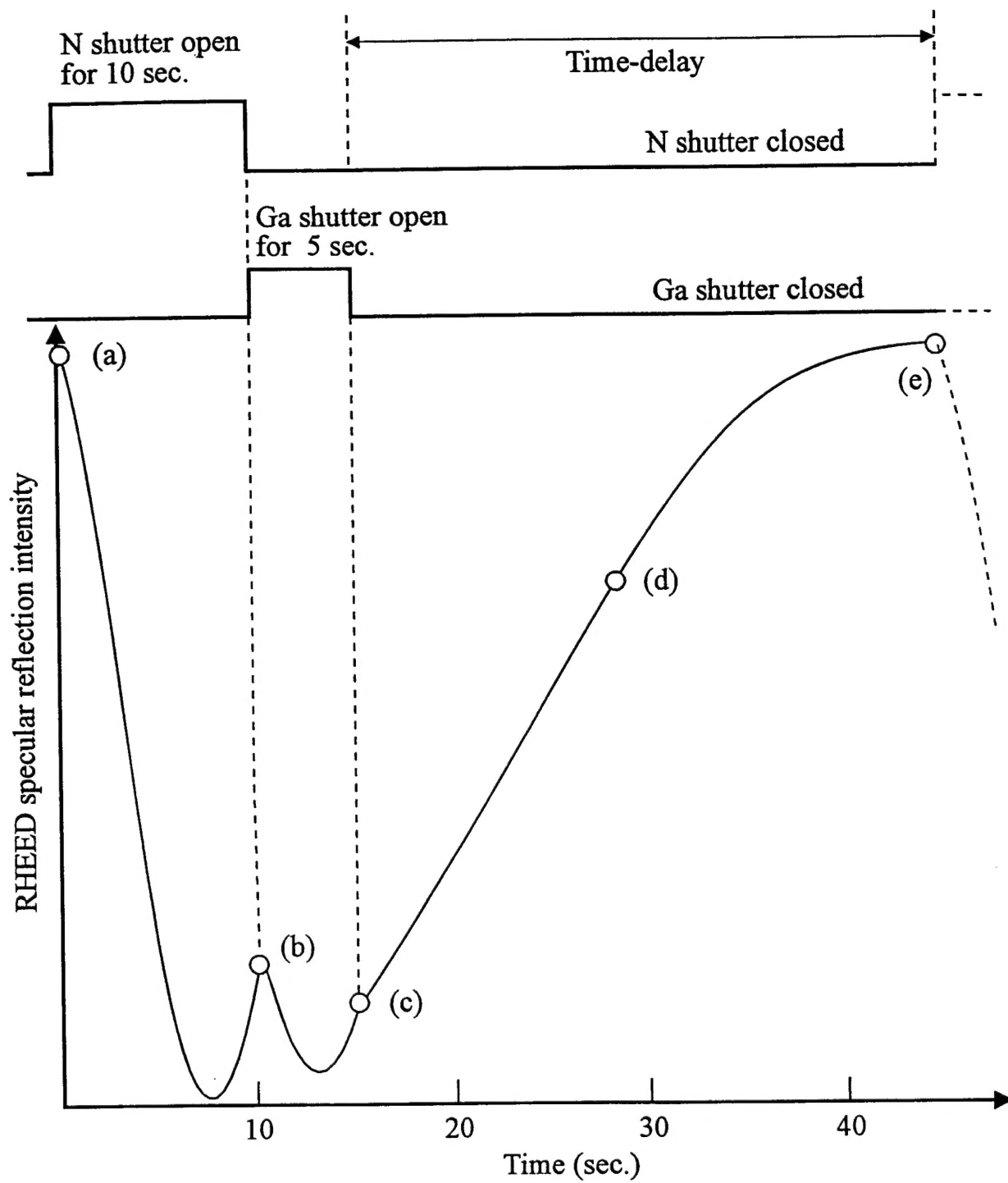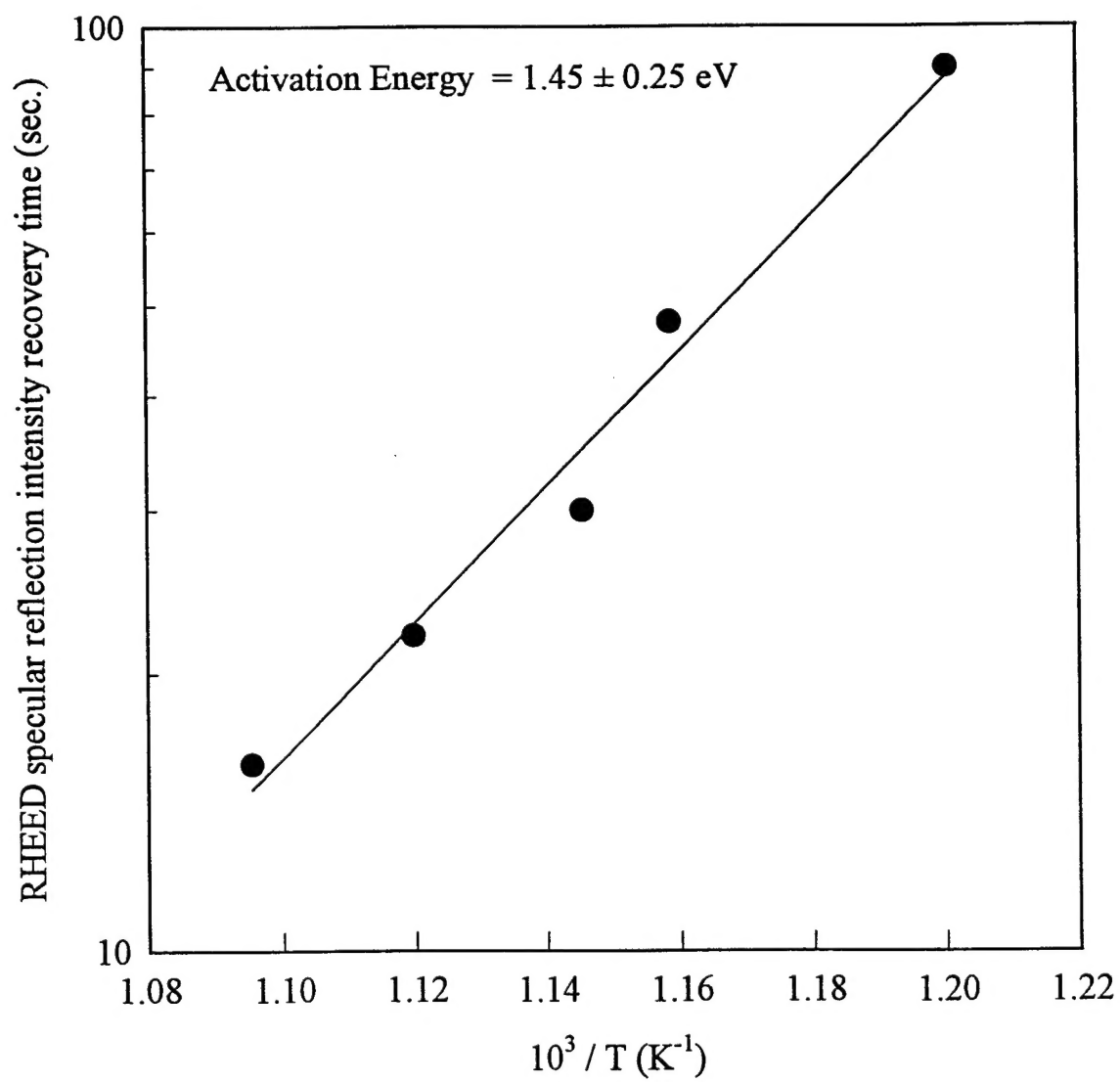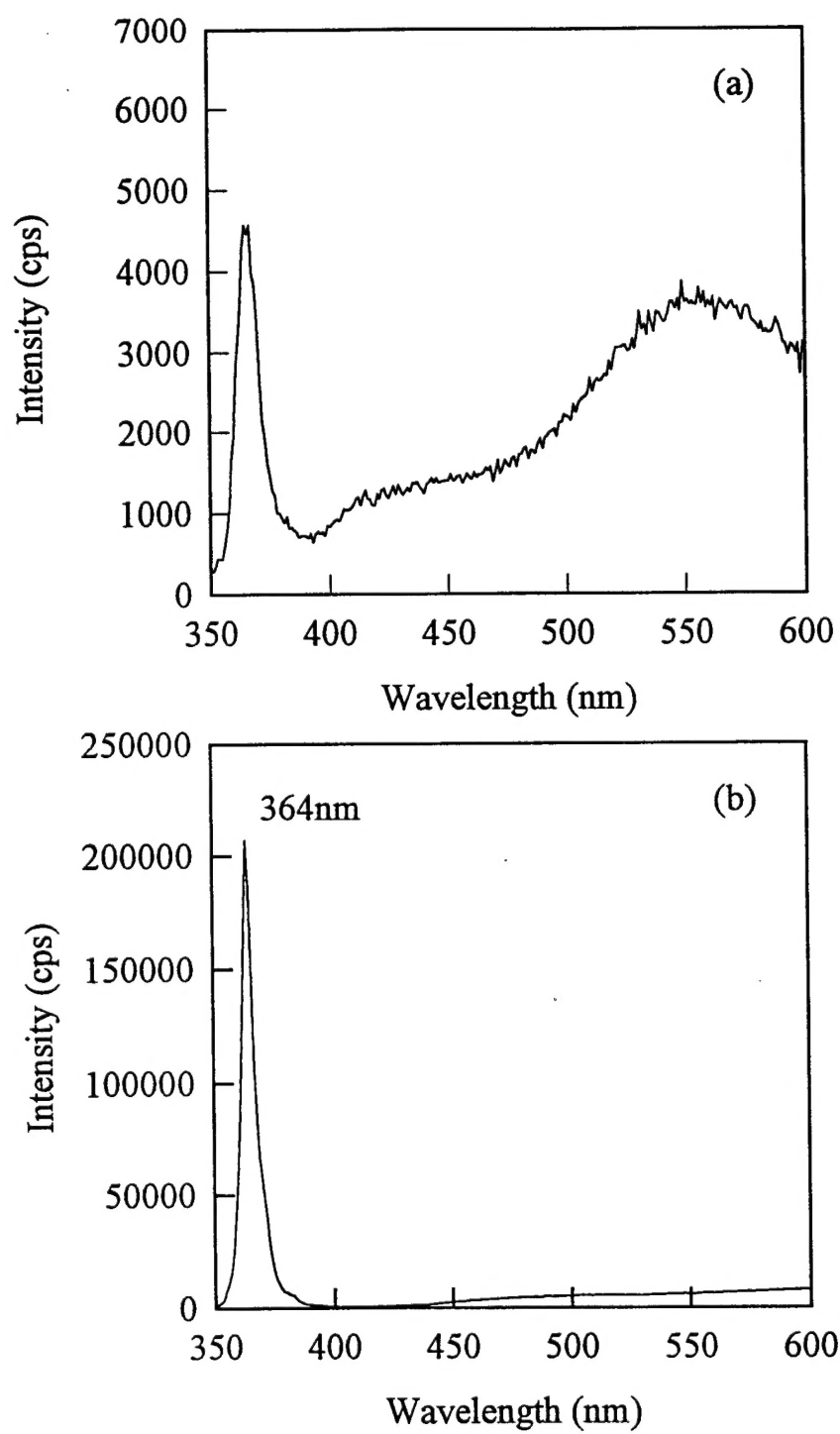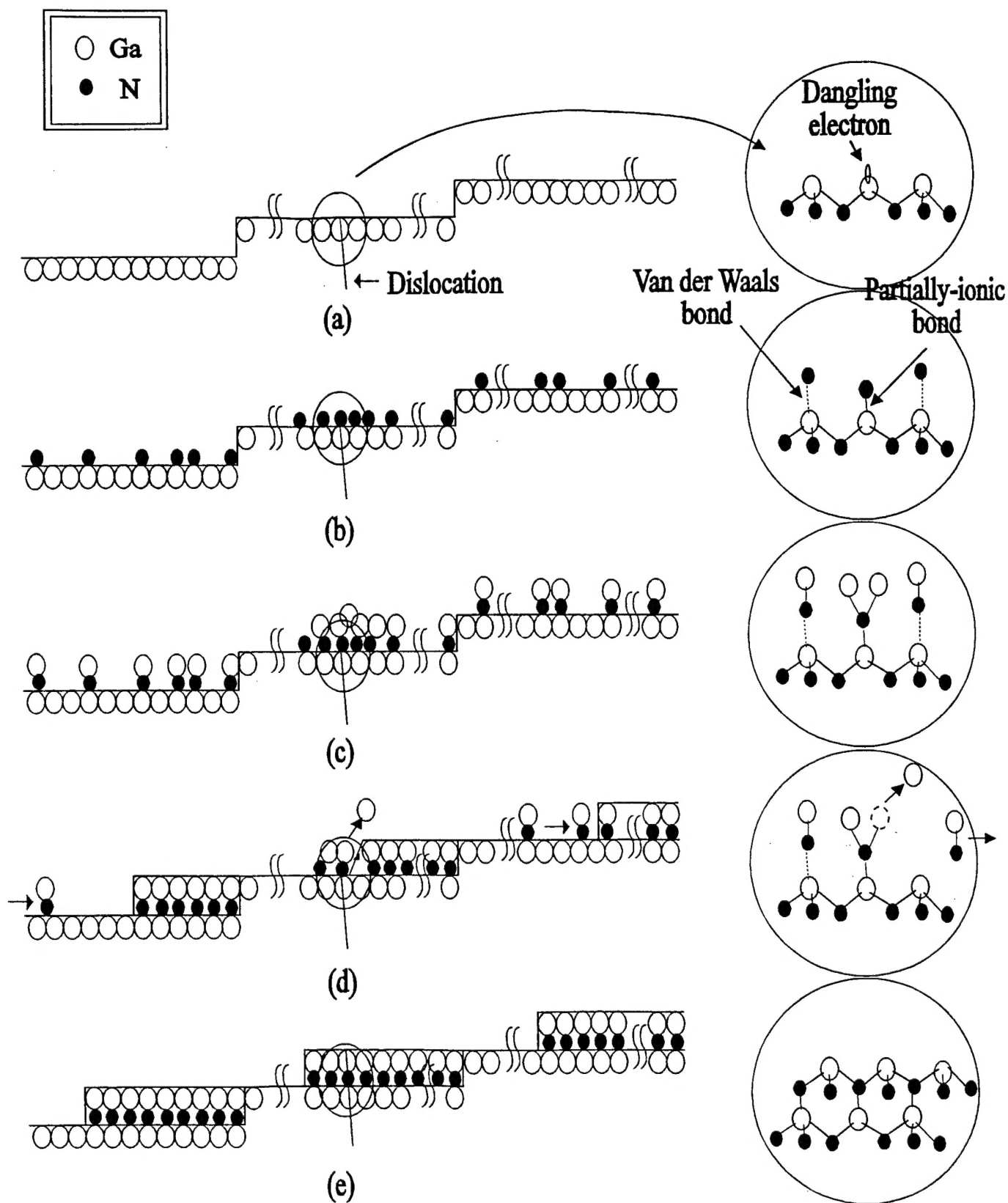Ga shutter closed

RHEED specular reflection intensity

(a)

(b)

(c)

(d)

(e)

10

20

30

40

Time (sec.)

Fig. 1

Fig. 2

Fig. 3

Fig. 4